國 立 交 通 大 學

光電工程研究所

碩士論文

氫氣/氖氣操作之尖端電極增強型

微電漿元件之特性研究

Characterization of nano-tip enhanced microplasma devices operated in argon and neon

研究生：吳正宇　　　　　　　Zheng-Yu Wu
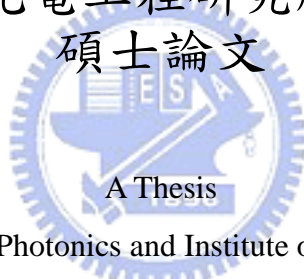
指導教授：金星吾 博士　　　　Dr. Sung-O Kim

中華民國 九十五 年 六 月

氬氣/氖氣操作之尖端電極增強型
微電漿元件之特性研究

Characterization of nano-tip enhanced
microplasma devices operated in argon and neon

研 究 生: 吳正宇　　　　　Student: Zheng-Yu Wu

指導教授: 金星吾　　　　　Advisor: Dr. Sung-O Kim

國立交通大學　電機學院
光電工程研究所
碩士論文

A Thesis

Submitted to Department of Photonics and Institute of Electro-Optical Engineering

College of Electrical and Computer Engineering

National Chiao Tung University

in Partial Fulfillment of the Requirements

for the Degree of

Master

in

Electro-Optical Engineering

June 2006

Hsin-Chu, Taiwan, Republic of China

中華民國九十五年六月

氫氣/氖氣操作之尖端電極增強型微電漿元件之特性研究

碩士研究生：吳正宇　　　　　指導教授：金星吾 博士

國立交通大學　　光電工程學系光電工程研究所

中文摘要

　　微電漿元件的研究近來提供了許多相當引人注目的特性與可能的應用。微電漿元件科技是結合電漿科學，光電科學與材料科學的一個新領域，並提供了電漿科學一個新發展空間。專門提供探討微電漿科技的研討會(IWM, International Workshop on Microplasmas)也在近年發展並漸有規模。目前在發展微電漿元件上有兩個主要的方向：(1)觀察電漿在微米尺寸與奈米尺寸之下的物理現象與光電特性，(2)發展不同結構與材料來使得微電漿可以與光電科技等不同領域作整合應用。

　　本篇論文闡述尖端電極增強型微電漿元件在氫氣/氖氣操作環境下的特性研究成果。在微電漿元件中採用尖端是希望利用其提升局部電場強化，進一步降低電漿崩解電壓。實驗包含建構一高真空系統以提供電漿操作環境、元件製程、量測電性與光學影像。經由實驗結果，穩定電壓電流特性、低操作電壓、大驅動裕度(Margin)、穩定輝光放電現象均可以由本研究之微電漿元件得到。本論文中所得到的元件特性展現尖端電極增強型微電漿元件與其他領域整合應用的充分潛力。

Characterization of nano-tip enhanced microplasma devices operated in argon and neon

Student：Zheng-Yu Wu　　　　Advisor：Dr. Sung-O Kim

Department of Photonics and Institute of Electro-Optical Engineering

National Chiao Tung University

Abstract

Recently, microplasma devices afford attractive properties and possible applications. The growth of the topical conferences on microplasma reveals the potential of development. Microplasma science and technology which is at the intersection of plasma science, photonics and materials science offers a new realm of plasma application. Two main tendencies in the development of microplasma devices: (1) to investigate the physics of ionized plasmas in micro or nano scale plasma devices, (2) to develop structural configurations and materials that allow microplasma to be integrated with electro-optical components.

The aim of this article attempts to characterize the nano-tip enhanced panel type microplasma device in argon and neon gases. The main idea for adopting nano-tips in the microplasma device is to enhance the electric field. Results of this study showed that abnormal current-voltage characteristics, low operating voltages, large voltage margins, and stable glow discharges can be observed by the proposed microplasma devices. To conclude, with the advantages from proposed device, the nano-tip enhanced microplasma technology provides possible opportunity to integrate with broad applications.

致謝

　　終於完成在交通大學兩年的碩士生也順利完成此論文，首先要感謝教授金星吾博士兩年來的指教，使我從這兩年艱苦歷練的歲月中了解到人生更多的面向；專業上，交大的良好研究環境也使我對微電漿元件與顯示器技術有更深入的瞭解。

　　在實驗室的兩年多日子裡，有苦也有樂，感謝李偉誠、卓龍材、任珂銳與周鴻杰四位一同打拼、酸甜與共的同袍，讓我在心情上得以抒發、實驗製程有同伴相陪、最愛的棒球也有夥伴，很高興這路上有你們陪伴相互砥礪，希望未來能夠延續這份情誼。感謝實驗室助理小姐張雅惠與何淑芳在各方面的協助與指導，感謝實驗室學弟林義淵帶來實驗室歡愉的氣氛，以及其他曾經幫助過我的學長、學弟與同學們，讓我順利渡過兩年碩士班的日子。　此外，我要感謝中華映管陳孝生處長在計畫上協助來完成微電漿元件之研究，還有交大顯示所王俊雄先生在研究設備採購過程中提供許多寶貴的意見。

　　最後，對於我的家人，特別是爸爸跟三位姊姊們，感謝你們在我學習路上這些年來對我的支持與照顧，使我能夠心無旁騖的專心於研究與學習。還有要感謝的是女友鄧安妘小姐，你跟我一同度過了這段重要的歲月，生活上的照顧與關懷，更讓我有力量度過次次的難關。現在我順利完成碩士學業即將離開交大，此刻我心中充滿喜悅，願將這喜悅與曾經關心與幫助我的朋友們分享。

Table of Contents

Figure Caption

List of Table

Chapter 1

Introduction

1.1 Background

The last decade have seen growing importance placed on research in microplasma device, and there has been a dramatic increase in the number of publications on microplasma devices. Recent developments in fabrication processes improved by the semiconductor technology provided a ladder to acquire non-equilibrium plasma with geometric dimensions as small as 10 μm [1]. Plasma sources with operating pressure close to atmospheric reveal many useful applications on atomic emission spectrometry, surface treatment, reduction of pollutants, and generation of UV radiation. The increased interest in direct current (DC) and pulsed corona discharge, dielectric barrier discharges, micro hollow cathode discharge, radio frequency and microwave discharges is due to the fact that for application on industrial field and it is very important to achieve high pressure operation with moderate operating voltage. The proposed nano-tip enhanced microplasma device can generate high pressure plasma up to 800 Torr at operating voltage of few hundreds volts. This thesis is devoted to the study of nano-tip enhanced microplasma devices operating in a wide pressure range from 300 to 800 Torr. Different gas content and various excitation frequencies were adopted to study electrical properties and optical appearances of the proposed microplasma devices.

1.2 Microplasma devices

The concept of microdischarge, introduced by A. D. White in 1959 [2] with the hollow cathode glow discharge phenomena, reveals its roots in the development of the first plasma display panel (PDP) by Bitzer and Slottow in 1966 [3]. In more recent years, Schoenbach et al. [4, 5] and Frame et al. [6] have consolidated the relish in the research of microdischarges. Fig. 1-1 shows the cavity cathode cross section of hollow cathode glow discharge device from design of A. D. White [2]. In February of 2003, Professor K Tachibana (Kyoto University) organized a workshop in Japan entitled "The New World of Microplasmas." which, for the first time, devoted an entire conference to the exciting scientific challenges and technological opportunities for microplasmas/microdischarges. Less than two years later (October 2004) Professor K. H. Becker, J. Gary Eden and K. H. Schoenbach hosted "The Second International Workshop on Microplasma (IWM-2004)" at USA. The growth of this series of microplasma conference shows the potential of microplasma device. With the intersection of plasma science, photonics and materials science, microplasma device science and technology offers not only a new realm of plasma application but also device capability [7-10].
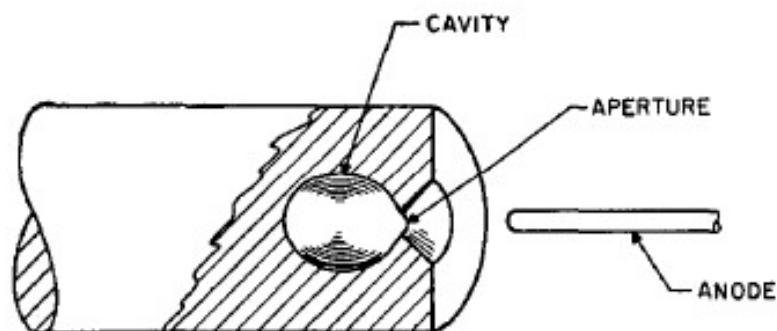
Fig. 1-1. Cavity cathode cross section of hollow cathode glow discharge device [2].

In University of Illinois at Urbana-Champaign, J. Gary Eden, the director of laboratory for optical physics and engineering, is offering a suite of microcavity plasma device fabricated in silicon, ceramic and metal/polymer structures. The simplest microcavity plasma device from University of Illinois at Urbana-Champaign is composed of an insulator sandwiched between two conductors. A microcavity of the conventional microdischarge device is formed by all sorts of different approaches through one of the conducting layers and the insulating layer, or through all layers. Fig. 1-2 shows the three conventional microcavity discharge device.
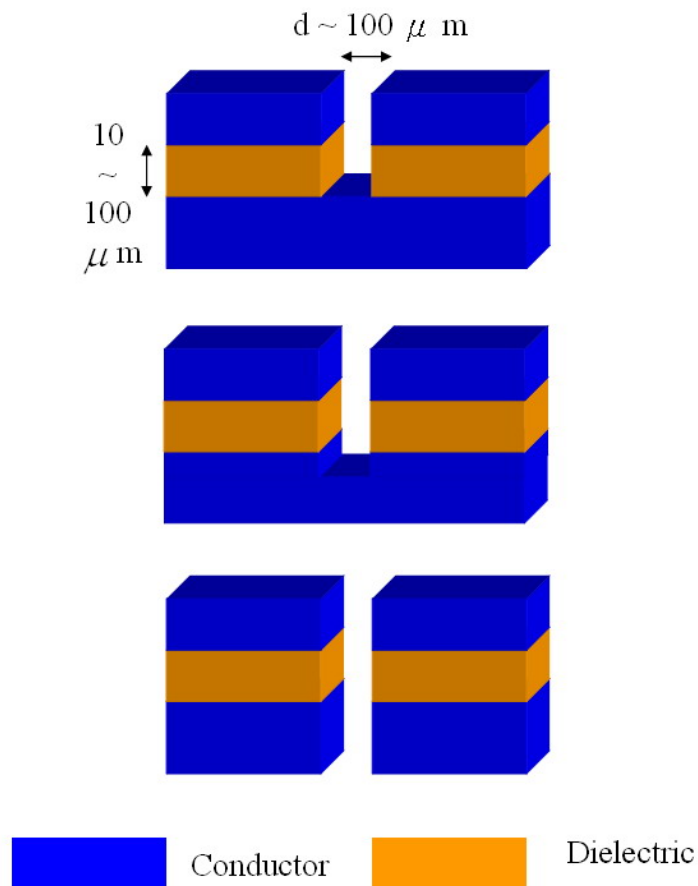
Fig. 1-2. Schematic side view diagram of typical microcavity discharge device.

Recently, J. Gary Eden's research team, the most active team on the field of microplasma device, developed 500 × 500 pixels microplasma devices with an overall active area of 25 cm^2. Fig. 1-3 shows the operated 500 × 500 microcavity plasma array fabricated on Si wafer [11]. In the demonstration of large (500 × 500) arrays of microcavity plasma devices in silicon, each pixels as small as (50 μm)^2 provide uniform emission which is better than ±10% across the entire array. Combining the concept of phosphor, bright light emission is produced when a 20 μm thick film of a green phosphor (Mn:Zn$_2$SiO$_4$) is screen printed onto a thin glass plate which mounted above a 500 × 500 arrays.

(a)   (b)

(c)
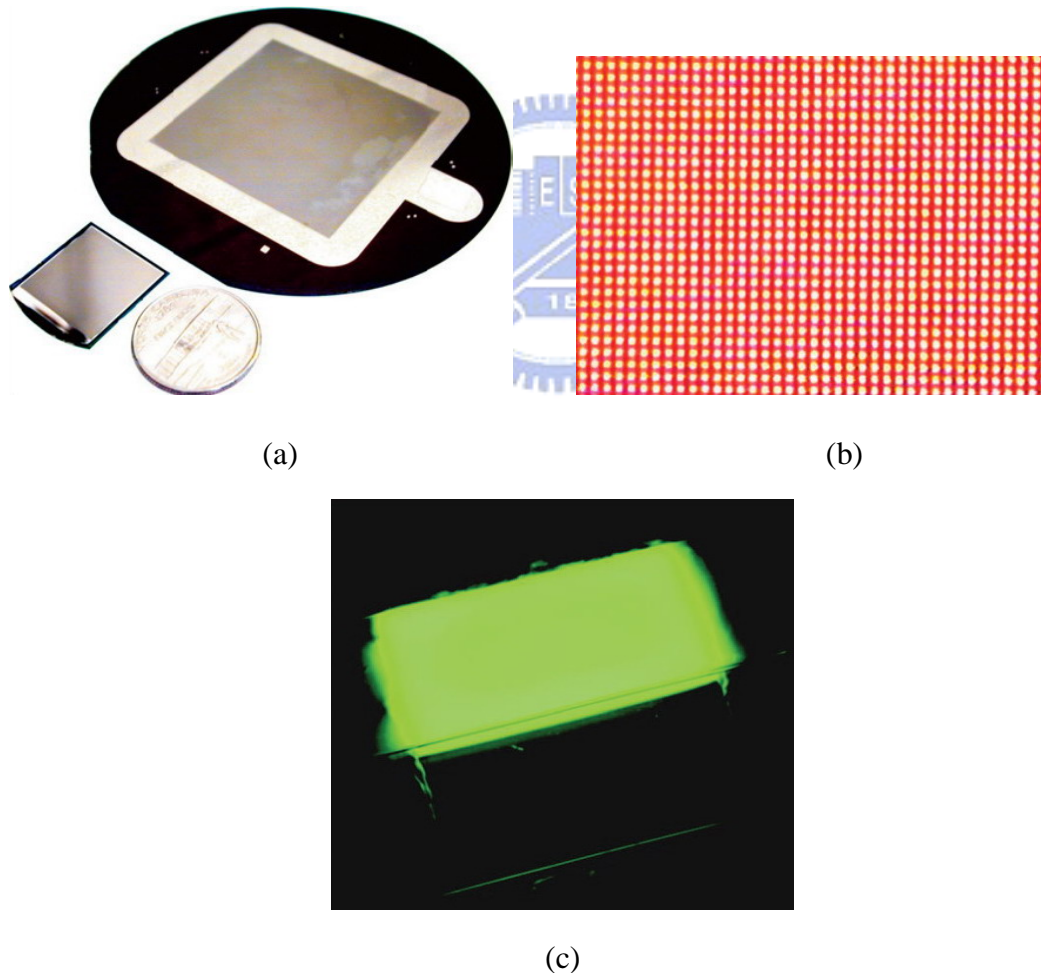
Fig. 1-3. Photographs of a 500 × 500 pixel microplasma array fabricated in a 50 mm Si wafer: (a) The finished device, (b) the array in operation in 700 Torr of neon, (c) green light emission from phosphor printed microplasma array [11].

In Frankfurt University, C. Penache proposed the micro structured electrode (MSE) sustained plasma device as shown in Fig. 1-4. The three-dimensional design is similar to above device from University of Illinois at Urbana-Champaign, but not the planar micro structured electrode plasma device. The discharge gap of the micro structured electrode array is down to sub millimeter scale and operating pressure could be increased to atmosphere level. Micro structured electrode arrays with discharge gap of hundreds of μm atmospheric pressure plasma can be generated at forward voltage of few hundreds volts. Based on micro structured electrode, stable homogeneous glow discharges can be operated in air, noble gases and mixtures containing reactive gases at pressures ranging from 40 to 760 Torr [12].
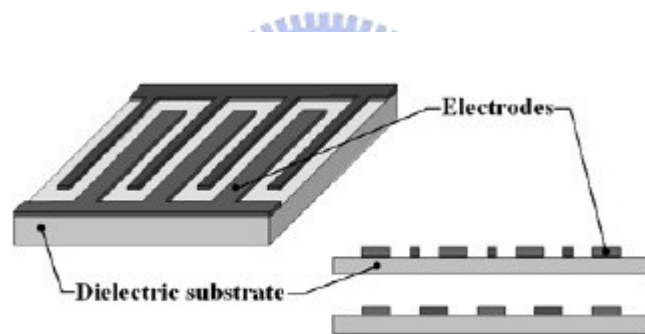
(a)
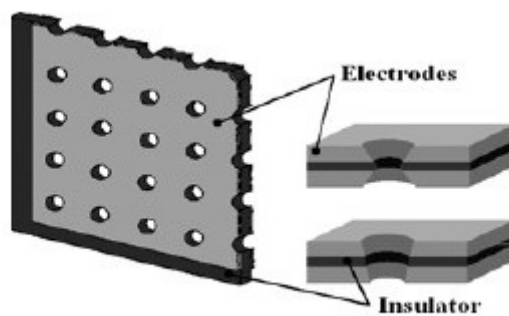
(b)

Fig. 1-4. Planar (a) and three-dimensional (b) micro-structured electrode device [12].

For microplasma devices, the typical cavity diameter or distance between electrodes is less than the order 1 millimeter. In the recent years, many research teams provide reduced these sizes to smaller dimensions by the photolithographic processes. Since the earliest structures were reported in the latter half of the 1990s, microplasma devices have been fabricated in several material platforms, including semiconductors, ceramics and multilayer metal/dielectric sandwiches, and the functionality available with these devices continues to expand to now. Fig. 1-5 shows diagrams of several electrode geometries of microcavity plasma devices [1]. Emission of above microdischarge devices is from the far infrared to the ultraviolet and operation is at pressure up to atmospheric.
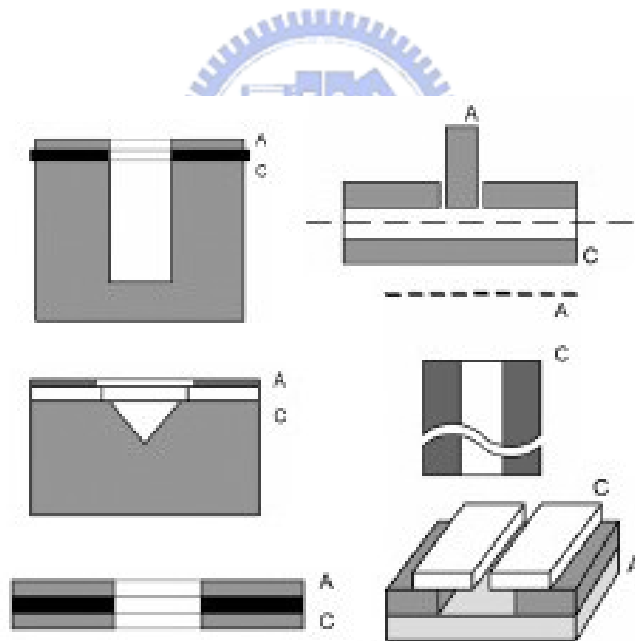
Fig. 1-5. Various geometric structures of microcavity plasma devices [1].

6

1.3 Motivation

As illustrated above, a fairly large body of literature exists on the silicon microdischarge device. It should be noted, however, the lack of literature reporting glass-based microdischarge device, which is suitable for big size development such as the application of liquid crystal display (LCD) backlight and planar plasma lighting source. The drawbacks in typical silicon microdischarge devices are the operating must be in a vacuum environment and the size of silicon wafer directly limits the size increase of the microdischarge devices. In addition, low operating voltages in glow discharge device can contribute to low power consumption. Therefore, a nano-tip enhanced panel type microplasma device with glass substrate was proposed to solve these issues. The characteristic of this design is to make use of glass substrate, whose size can be easily increased with expectation, to form a panel type microplasma device. Furthermore, the main idea for using nano-tip enhanced electrode is to locally enhance the electric field when a potential difference is applied on the electrodes. Low operating voltages, large voltage margin and stable glow discharge can be acquired in this configuration of nano-tip enhanced microplasma device.

The investigation of nano-tip enhanced panel type microplasma device with glass substrate is the purpose in this thesis. The advantages of proposed device are that it makes more desirable for size development than the conventional microdischarge devices and superior electro-optical properties can be acquired by the locally enhanced electric field with nano-tip.

1.4 Overview

This thesis is structured as follows. A brief introduction of gas discharge phenomena, i.e. plasma, will be described in **Chapter 2**. In **Chapter 3**, the fabrication processes of proposed device are presented. Furthermore, the experimental setup used to operate the device and characterization methods are illustrated. In **Chapter 4**, the collected data including current-voltage characteristic, operating voltages and voltage margin from discharges operating in argon and neon as filling gases are presented and discussed. **Chapter 5** summarizes the conclusions of this thesis and discusses the possible future works.

Chapter 2

Gas Discharges

2.1 Introduction

"Gas discharge" is a phenomenon that an ionized gas with electrical discharge, i.e. plasma. The main idea for using nano-tip is to locally enhance electric field while a potential difference is applied on the electrodes. While the differential potential is applied on the device in a gaseous medium, in the high field regions free electrons can be amplified in an avalanche process. When the external electric field exceeds a threshold value, the charge multiplication develops exponentially and a gas discharge is ignited. Secondary electrons are released also from the cathode surface, not only in the gas volume.

The second chapter presents the theory of glow discharge, gas breakdown, Paschen curves and Penning effect. The described knowledge can assist reader to understand the phenomena of proposed microplasma device. A deeper theoretical study of the microplasma devices and additional information of gas discharge can be derived from [13-17].

2.2 Glow Discharges

The glow discharge is one of the most studied and widely applied gas discharges. The name "glow discharge" is to the fact that plasma is luminous and the wavelength of the glow discharge depends on the gas used. Gas discharge (plasma) can be broadly defined as a system of electric neutrality composed of positive- and negative-charge particles. The degree of ionization may range from small as in the conventional glow discharge to very high as in the nuclear reactions. The first form of plasma observed was the positive column of the glow discharge, in which an equal number of positive ions and electrons. Gas discharge state is known as the fourth state of matter in the universe besides solid, liquid and gas state as shown in Fig. 2-1. The majority of the universe exists in a plasma state, including the stars, which are almost completely ionized with the high temperatures. Under normal state, a gas is mainly made up of uncharged particles and is almost a perfect insulator. While an electric potential of sufficient intensity is established in the gas between two electrodes, the gas can become to plasma state with an almost completely conducting state [17, 18].
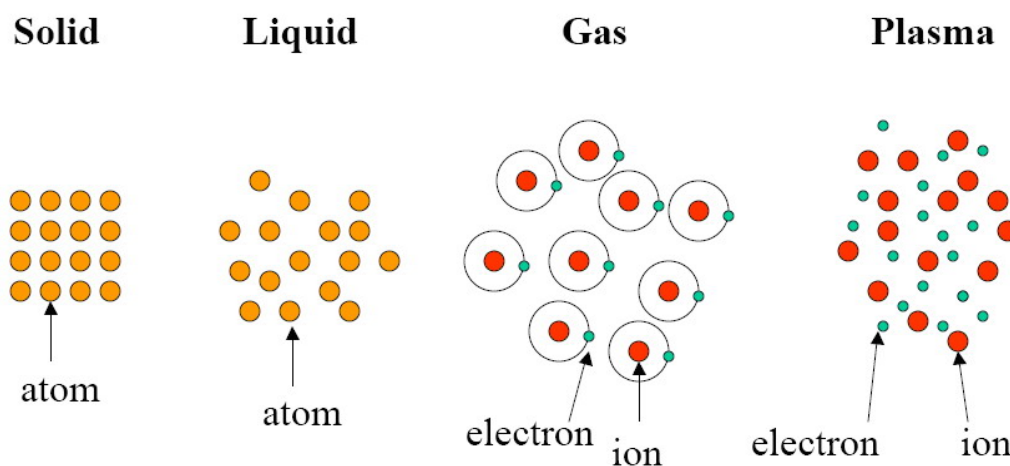
Fig. 2-1. Four kinds of matter state in the universe.

The operation condition of glow discharge is typically in a gas between two electrodes with large differential potential. The voltage distribution of glow discharge process is shown in Fig. 2-2. The potential drops rapidly close to the cathode, vary slowly in the plasma, and change again close to the anode. The distribution of electric fields is restricted to sheaths at each side of the electrodes. Electrons which try to reach electrode are repulsed by the sheath fields. Electrons originating at the cathode will be accelerated, collide, transfer energy, leave by diffusion and recombination, slow by the anode. Because the electrons have enough energy to generate light by excitation collisions, the luminous glow is produced. Since a continuous loss of electrons, the steady state must be maintained with an equal degree of discharge. The electrons absorb energy from the electric field, accelerate, ionize some atoms, and the processes are continuous. Secondary emission from the cathode produces additional electrons which are very important to maintaining a sustainable discharge.
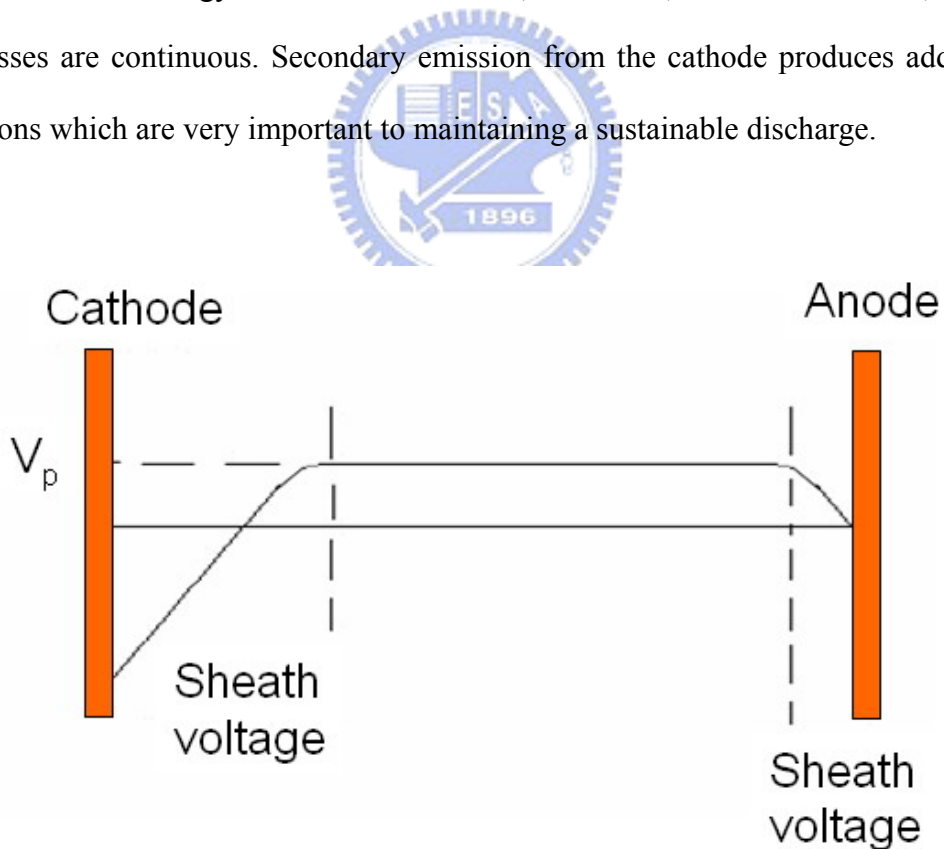
Fig. 2-2. Voltage distribution of dc glow discharge.

The sequence of layers, the distribution of brightness along the discharge tube and the potential distribution are shown in Fig. 2-3. For the conventional direct current discharge, the simplest type of glow discharge, the anode and cathode are made by metal conductor. The feature of this discharge is a layer of positive charge at the cathode, with strong field at the surface and considerable potential drop. This potential drop is named as cathode fall, and the thickness of the cathode layer is inversely proportional to the pressure of the gas state [14, 19].
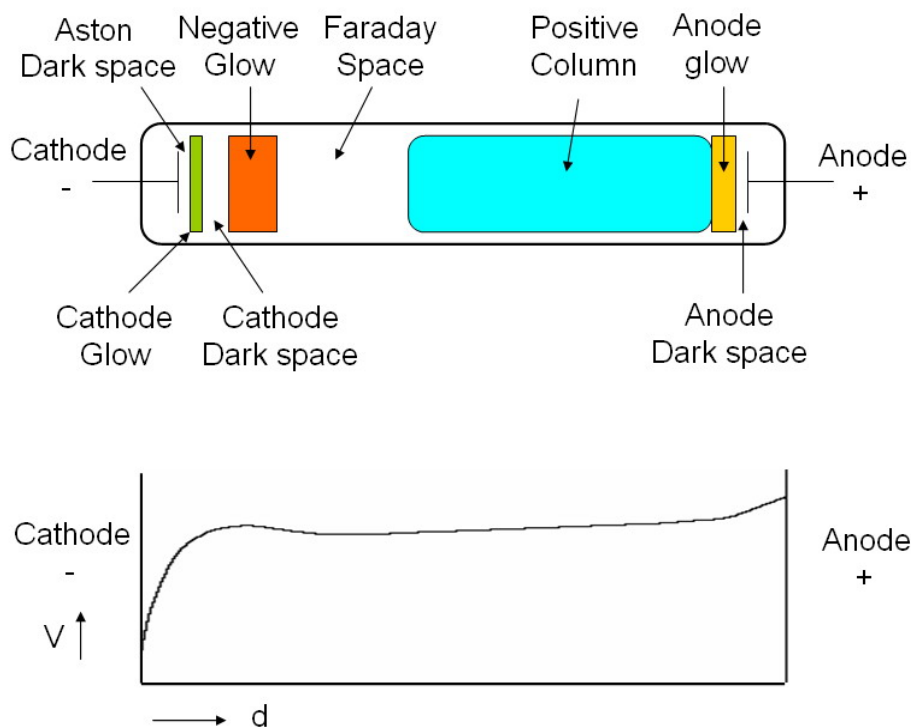
Fig. 2-3. Typical dc glow discharge distribution of brightness and potential.

Aston Dark Space is a thin region to the right of the cathode with a strong electric field. This region has a negative space charge, meaning that stray initial electrons together with the secondary electrons from the cathode outnumber the ions

in this region. The electrons are too low density to excite the gas, so it appears dark. There is an intense electric field in the cathode fall region, and the electric filed accelerates ions to the cathode. From the ion bombardment of the surface of the metal, free electron is generated and accelerated through the cathode fall region and toward the negative glow. With considerable exciting collisions, the negative glow is the most intense part of the discharge distribution. Therefore, the negative glow region is widely used in many applications such as plasma display panel (PDP). The negative glow has relatively low electric field, long, compared to the cathode glow and is the most intense on the cathode side. While the distance between electrodes is sufficiently large, an electrically neutral plasma region is formed between the cathode and anode. In the faraday dark space region, the electron number density decreases by recombination and diffusion to the walls, the net space charge is very low, and the axial electric field is small. Right to the faraday dark space region, there is a quasi-neutral region, positive column. The electric field of the positive column is just large enough to maintain the degree of ionization at its cathode end. The positive column is a long, uniform glow, except when standing or moving *striations* are triggered spontaneously. The acceleration and collision processes homogeneously repeat through the complete length of the positive column and form the uniform glow discharge. Between positive column and anode sheath, the anode glow region is formed. The anode glow region is slightly brighter than the positive column region. The anode dark space or anode sheath is a space between the anode glow and the anode. Due to electrons traveling from the positive column to the anode, there is the negative space charge in anode sheath.

The *striations* mentioned above means the traveling waves or stationary perturbations in the electron number density which occur in partially ionized gases. In

their usual form moving striations are propagating luminous bands which appear in positive columns. Standing striations can be easily photographed. Many apparently homogeneous partially ionized gasses in reality have moving striations. *Striation* is known in positive column and ionospheric plasma system, and it is associated with the wave related mechanism. *Striation* in typical dielectric microdischarge device predominantly occurs near the region and is basically governed by the ionization-dominated α-process [16].
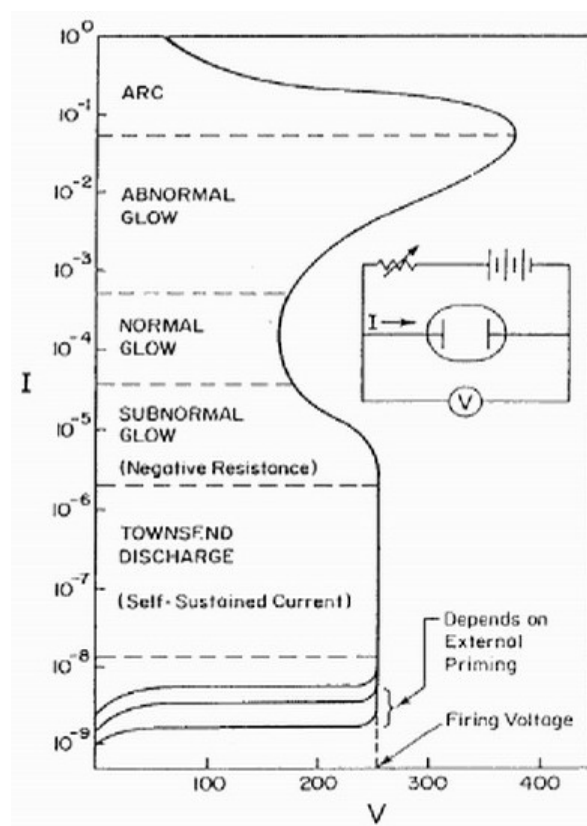
Fig. 2-4. Current-voltage (I-V) characteristic of discharge.

When gas breakdown occurs, the gas state becomes conductive from non-conductive. Change in the applied voltage can cause the variation of current and voltage in the discharge. A current-voltage (I-V) characteristic for a glow discharge

can be obtained by these measured parameters. A conventional current-voltage (I-V) characteristic of discharge is shown in Fig. 2-4. At low currents, the discharge is weakly ionized, characterized by high voltages and large resistance, and is referred to as a Townsend discharge. Increasing the current will cause a decrease in voltage until a minimum is reached, and this section is the normal glow where the discharge voltage is relatively constant with current variation. The positively sloped I-V trace is the abnormal mode of the discharge. When the cathode is completely covered by the discharge, the current is increased by increasing the voltage to supply more electrons to the discharge. Further increase in the current will result in a sudden drop in voltage and transition of the discharge to an arc state.

2.3 Breakdown of gases and Paschen curve

The phenomenon of gas breakdown in discharge device is the process of transformation from a non-conducting state to a conducting state. When the applied potential is low, the gas likes a near-perfect insulator. While the associated potential reaches the breakdown potential, the considerable ionization values make the gas breakdown with a light emission. During the gas breakdown process, the electron avalanche is a critical constituent first of all. An avalanche develops in the gas with a small number of seed electrons which may appear unexpectedly, and it even can be triggered by a single electron.

Gas breakdown is essentially a threshold process which means the breakdown formed with the electric field exceeds a specific value. The applied voltage across the electrodes is gradually increased from the initial state, and there is no change of the gas state. However, a critical value of applied voltage can suddenly make the ionization rises rapidly. The threshold process is consequence of steep dependence of the atomic ionization by electron impact on field strength and by the fact that ionization, producing electron multiplication, is accompanied by mechanisms that create obstacles to the development of the avalanche. After breakdown, the plasma can be sustained with a mechanism for the generation of ions and electrons to replace the loss of those.

The electron avalanche generated in a dc field forms in time and space. To characterize the rate of ionization, an ionization coefficient α cm^{-1} is led in, that is, the number of ionization phenomena performed by an electron in a 1 cm path along the field. The change in the number of electrons per unit length in the avalanche is proportional to the number of electrons at x by an ionization coefficient α. The number of electrons in the avalanche grows towards the anode can be shown as the

following Equations.

$$\frac{dN}{dx} = \alpha N_x \qquad (2.1)$$

$$N(x) = N_0 \exp(\alpha x) \qquad (2.2)$$

From above Equations (2.1) and (2.2), the electron current at the anode is

$$i = eN_0 \exp(\alpha d) = i_0 \exp(\alpha d) \qquad (2.3)$$

where d is the electrode separation. An electron leaving the cathode generates $\exp(\alpha d) - 1$ positive ions in the electrode separation. Each of the $\exp(\alpha d) - 1$ positive ions knocks out γ_i electrons from the cathode; γ_i is the secondary emission coefficient for the cathode. The electronic part of the cathode current i_1 is given by the equation,

$$i_1 = i_0 + \gamma_i i_1 [\exp(\alpha d) - 1] \qquad (2.4)$$

With secondary emission taken into account, the current at the anode and in the external circuit is

$$i = i_1 \exp(\alpha d) = \frac{i_0 \exp(\alpha d)}{\{1 - \gamma_i [\exp(\alpha d) - 1]\}} \qquad (2.5)$$

The secondary emission is caused by ions, photos and metasatable atoms. While the applied voltage between the electrodes $V > Vt$, the denominator ($\gamma_i [\exp(\alpha d) - 1]$)

17

in the Equation (2.5) is negative. The negative sign presents that the current cannot be steady at $V > Vt$. However, the current at $V < Vt$ with $\gamma_i[\exp(\alpha d)-1]>1$ is steady and non-sustained. The transition between above two situations is

$$\gamma_i[\exp(\alpha d)-1]=1 \tag{2.6}$$

Equation (2.6) shows a steady self-sustained current in a homogenous electric field $E_t = V_t/d$.

The breakdown voltage, V_t, can be expressed as an equivalent term, and it depend on the gas, the material of the cathode, the working pressure and the discharge gap of electrodes. A conventional empirical expression of first Townsend coefficient as follow

$$\alpha = A \cdot p \exp(^{-B \cdot p}\!/_{E}) \tag{2.7}$$

where constants A and B are determined by the experimental curves, E is the electric field strength and p is the working pressure. From the combination of Equations (2.6) and (2.7), we can acquire the breakdown voltage,

$$V_t = \frac{B(pd)}{\ln\left(\dfrac{A}{\ln(^{1}\!/_{\gamma}+1)}\right)+\ln(pd)} \tag{2.8}$$

It is obvious that the breakdown voltage depend only on the product pd. The constants A and B are related to the Equation (2.7). A and B are normally determined

experimentally for the specific gas over a range of pressure. Consequently, the breakdown voltages of each gas depend on the *pd* for a specific gas and the material of electrode. The constants A and B determined with experimental method shown in Table 2-1 [13].

Table 2-1. Constants A and B for the ionization and region of applicability [13].

Gas	A	B	E/p
	$cm^{-1}Torr^{-1}$	$V \cdot cm^{-1}Torr^{-1}$	$V \cdot cm^{-1}Torr^{-1}$
He	3	34	$20 \sim 150$
Ne	4	100	$100 \sim 400$
Ar	12	180	$100 \sim 600$
Kr	17	240	$100 \sim 1000$
Xe	26	350	$200 \sim 800$
Hg	20	370	$150 \sim 600$
H_2	5	130	$150 \sim 600$
N_2	12	342	$100 \sim 600$
CO2	20	466	$500 \sim 10000$
Air	15	365	$100 \sim 800$

Moreover, the values of secondary electron emission coefficients for tungsten and molybdenum in rare gases are shown in Fig. 2-5 [20] and the information about the value of secondary emission coefficient for metal the slow ions are shown in Table 2-2.
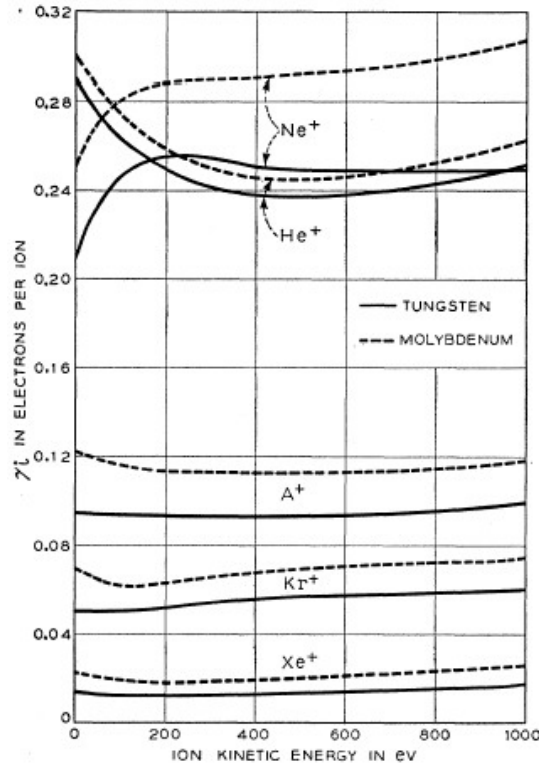
Fig 2-5. Secondary electron emission coefficient for the noble gas ions on clean tungsten and molybdenum.

Table 2-2. Value of secondary electron emission from metals for slow ions.

Metal	Ar	H2	Air	N2	Ne
Al	0.12	0.095	0.021	0.1	0.053
Ba	0.14		0.1		0.14
C		0.014			
Cu	0.058	0.05		0.025	0.066
Fe	0.058	0.061	0.015	0.02	0.059
K	0.22	0.22	0.17	0.077	0.12
Mg	0.077	0.125	0.031	0.038	0.089
Ni	0.058	0.053	0.019	0.036	0.077
Pt	0.058	0.02	0.01	0.017	0.059

Substituting the secondary electrons emission coefficient in Table 2-1 into breakdown voltage in Equation (2.8), a set of experimental curves $V_t(pd)$ is acquired in Fig. 2-6 [13].
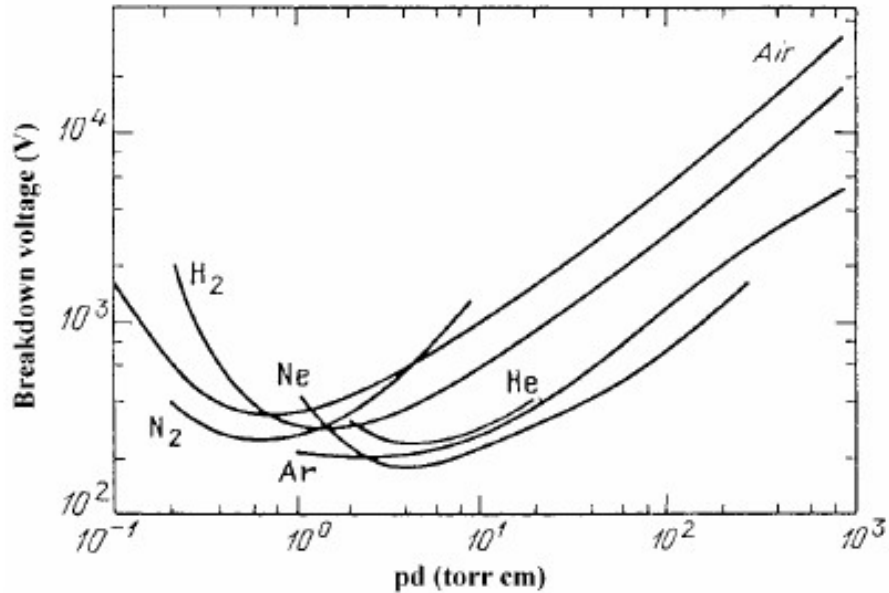
Fig. 2-6. Paschen curves: Breakdown voltage in various gases with different *pd* product values.

The curves in Fig. 2-6 known as *Paschen curves* provide the relationship between *pd* and the breakdown voltage. There is minimum voltage, $(pd)_{min}$, for each curve. At the Paschen minimum the discharge maintains itself with a minimum cathode fall voltage V_c and minimum power dissipation. In the normal glow discharge, the current density flowing to the cathode remains approximately constant as the total current varies, as the total area of contact with the cathode increases with the total current. In the region of large *pd*, right side of minimum, high pressures or large gaps reveal that an electron can produce numerous ionization collisions even at high E/p

and there are many collisions with high pressure or large gap. However, in the region of left side of minimum, the possibilities of collision processes are very limited. The dimensions of microplasma devices are at small level, hence the minimum breakdown can be acquired with high working pressure up to 1 atm.

2.4 Penning effect

Electron-impact ionization is the major source for charged-particles generation in a glow discharge [18]. Moreover, another important ionization mechanism is the direct ionization by collusion with sufficiently energetic, metastable neutral particles. This process is known as the *Penning ionization* and become the major mechanism with noble gases, such as Ne and Xe, are used as the gas content in plasma display panel (PDP).The probability of collisions involving excited atoms depends on the density of the excited atoms, and hence on their life time. Some excited atoms have very long lifetimes and these are known as metastable excited atoms; they arise because the selection rules forbid relaxation to the ground state, or in pratice, make such a transition rather unlikely. All the noble gases have metastable states, such as the metastable state of argon is at 11.55 eV [14].

A *Penning gas mixture* consists of a rare gas containing impurity atoms possibly at very low concentrations. The impurity atoms have an ionization potential which is lower than or equal to the metastable potential of the parent noble gas. The *Penning effect* in a *Penning gas mixture* is the ionization by charge transfer (charge exchange) during collision between a metastable atom and a neutral atom which decreases the average energy to form an ion pair. When a metastable atom collides with a neutral, the neutral can become ionized if its ionization energy is less then excitation energy of the excited atom, then the process

$$A* + G \rightarrow G^+ + A + e^-$$ (2.9)

is known as *Penning Ionization* and the related process

$$A* + G \rightarrow (A\,G)^+ + e^- \qquad\qquad\qquad (2.10)$$
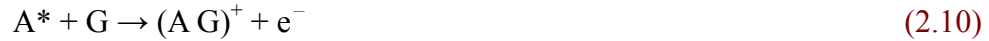
is called *Associative Ionization* (AI).

In a glow discharge, this results in an increase of the ionization coefficient (Townsend first coefficient), a decrease in breakdown potential and a lowering of the cathode fall potential. Coburn and Kay (1971) demonstrated the Penning ionization effect by sputtering a europium oxide target containing a small of iron, in both neon and argon discharges. Eu^+ (5.7 eV) and Fe^+ (eVi=7.8 eV) were observed in both gases, but O^+ (eVi=13.6 eV) was observed only in the neon discharge. Argon metastable is at 11.55 eV, whereas neon metastable is 16.62 eV [14]. Table 2-3 shows the ionization potential in penning gas mixtures of noble gases and mercury.

Table 2-3. Penning mixture of noble gases and mercury

Ionization			Penning mixture
Gas	First ionization energies	Metastable energies	Suitable penning additives
	eV	eV	
Helium	24.6	19.8	Ar, Kr, Xe, Hg
Neon	21.6	16.62	Ar, Kr, Xe, Hg
Argon	15.8	11.55	Hg
Krypton	14	9.9	
Xenon	12.1	8.3	
Mercury	10.4	4.7	

Chapter 3

Experimental Technologies

The fabrication technologies utilized to fabricate the proposed nano-tip enhanced microplasma devices will be firstly described in this chapter. The fabrication technologies by VLSI semiconductor process include photolithography, sputtering, and lift-off technology. A very high vacuum system, which is used to prepare a vacuum environment with base vacuum level 10^{-7} Torr and ignite the microplasma with excepted pressure of filled gas, will be depicted then. Followed by the description of the instruments, such as electric pulsed power source set and image observation system, for characterizing current-voltage characteristics, discharge voltages, voltage margin and optical appearance of a proposed microplasma device.

3.1 Introduction

The fabrication technologies of microplasma devices are getting more and more advanced. With the development of VLSI (Very Large Scale Integration) semiconductor fabrication processes, smaller and precise structure and electrode gap becomes possible to be fabricated.

A schematic diagram of the fabricated nano-tip enhanced microplasma device structure is shown in Fig. 3-1. The structure of the nano-tip enhanced microplasma device can be separated into two parts, front panel and rear panel. Front panel part including transparent indium tin oxide (ITO) electrode is fabricated by the

photolithography process and rear panel include metal electrodes with sputtering deposition and nano-tip with specific attachment process. A vertical discharge scheme with front transparent ITO electrode and rear metal electrode has been formed in the devices. The front transparent ITO electrode has been fabricated by the photolithographic techniques and the wet etching processes. The thickness and the sheet resistance of the ITO electrode are 1000 Å and 50 $\Omega/\square$. The sputtering deposition method was used to deposit the rear metal electrode with a thickness of 1000 Å. After front and rear panels, a sealing process is carried out to finalize the panel type microplasma devices. In addition, a nano-tip with a tip radius below 25 nm which coated with aluminum layers of 30 nm in thickness is attached on the rear metal electrode by the silver paste (4922N, DuPont). With specific spacers, the sealing processes of exhausting tube and panels have been achieved by vacuum sealant (VARIAN) by a temperature curing process to finalize the panel type devices. The specifications of fabricated devices are offered in Table. 3-1.
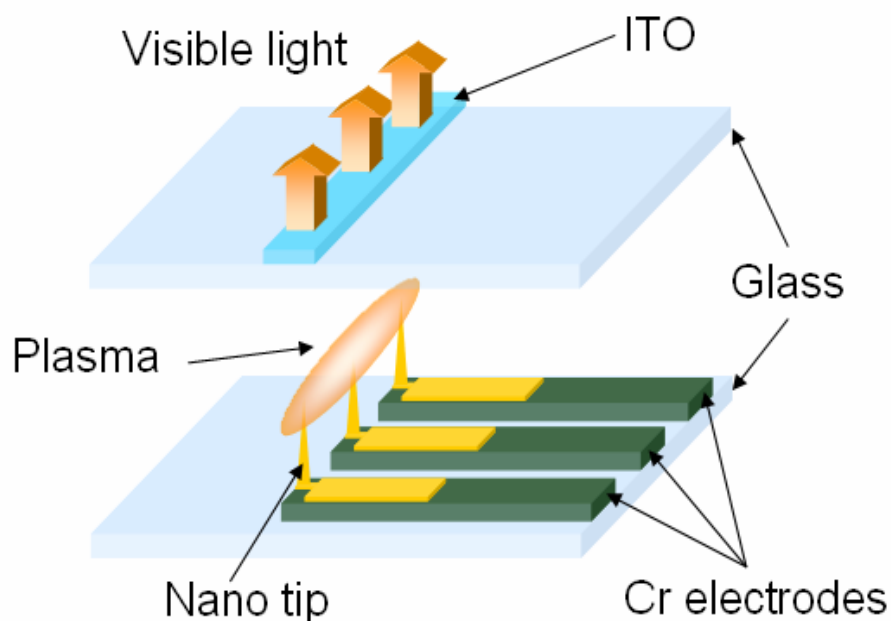
Fig 3-1. Schematic diagram of the nano-tip enhanced microplasma device.

Table 3.1. Specifications of fabricated microplasma devices

	Material	Thickness or Condition
Front substrate	ITO glass	1 mm
Front electrode	ITO	1000 Å
Rear substrate	Soda-lime	2 mm
Rear electrode	Cr	1000 Å
Spacer	Soda-lime	400 μm
Gas content	Ne, Ar, Ne+Ar(2%)	300 ~ 800 Torr
Driving	Bipolar pulse	2 ~ 20 kHz

The experimental arrangement designed for the measurement is schematically shown in Fig. 3-2. The experimental arrangement consists of a vacuum system, a gas filling system, a pulsed power source set and an image observation system. The vacuum system has been evacuated with residual pressure lower than 10^{-7} Torr by a turbomolecular pump (Leybold Vacuum). The gas filling to make the base vacuum grade from 300 to 800 Torr are neon (Ne), argon (Ar) and Ne+Ar (2%). The direct current bipolar pulsed excitation waveform, having the duty ratio with 20%, was applied with the frequency from 2 to 20 kHz between the front ITO electrode and the rear metal electrode by the pulse DC power controller (SHENCHANG ELECTRIC, SPIK 2000A).

The electrical properties of the microplasma devices, such as current-voltage characteristics and discharge voltages of microplasma, were measured with typical electrical instruments. The color charged-coupled device (CCD) images and photographs were caught by an image observation system which is composed of a color charged-coupled device (CCD) camera (Watec, WAT-202D), a zoom lens set

27

(Navitar, Zoom 6000), a digital camera and a personal computer. We shall describe

the major features of the above mentioned technologies in this chapter.
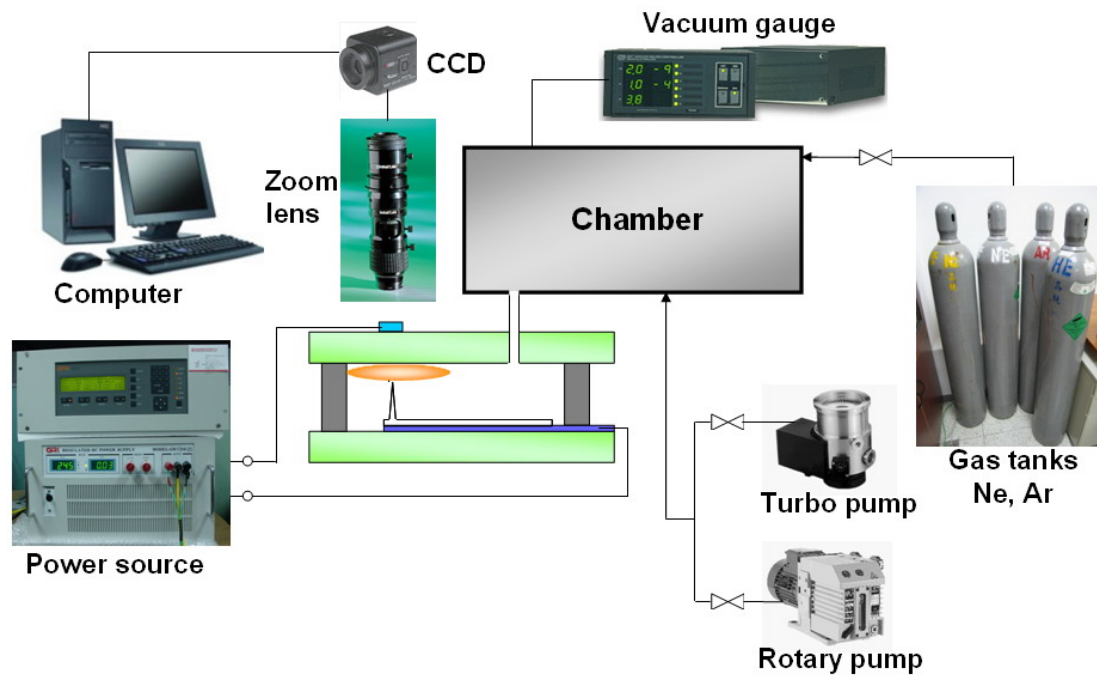
Fig. 3-2. Schematic diagram of the experimental arrangement.

3.2 Device fabrication

3.2.1 Substrate preparation

The proposed nano-tip microplasma device is a panel type configuration. Therefore, indium tin oxide (ITO) coated glass and the conventional soda-lime glass were used as the substrates. Because of the essentials of transparency in the front panel, the ITO glass was selected as the front substrate. Otherwise, the rear substrate adopts a soda-lime glass to deposit metal electrodes with sputtering method. For panel type microplasma devices, the gas exhaust hole on a glass substrate should be provided. Therefore, a mechanical drilling method has been used to make the gas exhaust hole on soda-lime glass.

First step is an initial cleaning. The cleaning condition of the surface of these two glass substrates could affect the following processes and the characteristics of device. Wet cleaning processes are necessary to obtain an ultra clean surface for subsequent fabrication. Consequently, a glass surface cleaning process has been adopted in an ultrasonic cleaner as shown in Fig. 3-3.

This cleaning process of glass surface is shown as following procedures:

(1) Rinse, clean the glass in ultrasonic cleaner with deionized (DI) water, 5 min.

(2) Rinse, clean the glass in ultrasonic cleaner with acetone (ACE), 5 min.

(3) Rinse, clean the glass in ultrasonic cleaner with isopropyl alcohol (IPA), 5 min.

(4) Rinse, clean the glass in ultrasonic cleaner with deionized (DI) water, 5 min.

(5) Rinse, clean the glass in ultrasonic cleaner with isopropyl alcohol, 5 min.

(6) Dry, dry the glass with nitrogen gas blowing.

Fig. 3-3. Ultrasonic cleaner for glass substrate cleaning.

3.2.2 ITO electrode patterning

The fabrication processes to pattern the ITO electrode include photolithography, and etching is similar to VLSI fabrication processes. We implement our fabrications in the Nano Facility Center (NFC) at National Chiao Tung University (NCTU). First we plot the electrode pattern, and then generate the pattern to a photo mask in a laser pattern generator. The third step is the VLSI lithography/etching process to produce the desired ITO electrode pattern.

Photolithography process is extensively used in Very Large Scale Integration (VLSI) or microelectromechanical (MEMS) fabrication technologies, and it can transfer the pattern of a mask to photoresist (PR). To prevent the PR peel off substrate during the developing or etching processes, hexamethyldisilazane (HMDS) is widely used in the semiconductor industry to improve photoresist adhesion. A photoresist typically consists of three components: resin, solvent and sensitizer. Resin is a binder

that provides mechanical properties to be the etching mask, sensitizer is photoactive compound that govern the sensitivity of PR, and solvent can keep the resist liquid and adjust the viscosity of PR. Because of the transparency of ITO conducting glass, we choose it to be the front panel substrate in our device. In general, the transparent conducting film for electrode in flat panel display is fabricated by sputtering with indium tin oxide (ITO) target. At the previous section, the cleaning processes of glass surface have been introduced. After cleaning, the VLSI lithography/etching processes have been carried out to fabricate the ITO electrode pattern.

The lithography/etching processes is described as follow. Firstly, HMDS layer is coated in the vacuum oven to improve photoresist adhesion after surface cleaning. The coating of photoresist will be applied after HMDS layer. The glass is placed on a vacuum chuck in the coater and the photoresist, FH6400, is dropped onto the center of the glass. A uniform and thin photoresist layer can be coated on the glass surface after spinning the glass subtrate. The parameters of positive photoresist, FH6400, are shown in Table 3-2. Third step is exposure and the mask pattern is then transferred onto the glass by the mask aligner (MJB-3, Karl-Suss) as shown in Fig. 3-4 (a). After exposure, the exposed glass is immersed in the developer, FHD5. Therefore, the desired pattern will show up in the photoresist. Chemical wet etching process is then carried out to transfer the developed photoresist pattern to the ITO layer. Wet etching is an isotropic etching, because the etchant have a same etching rate in all directions. Regions not covered by the photoresist are removed during the wet etching process. The remained photoresist are then stripped by acetone (ACE) and the desired ITO pattern is represented. After developing, the completeness of ITO pattern is investigated by an optical-microscope as shown in Fig. 3-4 (b).

Table. 3-2. Parameters of FH6400 in the photolithography for ITO electrode patterning.

| FH-6400	
Type	Positive PR
Rotation speed and time	1st: 1500 rpm, 20 sec.
	2nd: 4000 rpm, 50 sec.
Soft bake	90 ° C, 80 sec.
Hard bake	120 ° C, 100 sec.
Exposure	150 sec.
Develop	90 sec.
Rinse	240 sec.
Thickness	1.5 μm

Fig. 3-4. Schematic diagram of aligner (left) and optical microscope (right).

The detailed description of the photolithography is provided as follow:

(1) HMDS and bake, coat a HMDS layer on surface and bake with 150° C in

a vacuum oven.

(2) Photoresist (PR) spin coating, place the substrate on a vacuum chuck in the coater and drop appropriate PR, FH6400, on the center of the glass substrate: first step with 1000 rpm, 20 sec and second step with 4000 rpm, 50 sec.

(3) Soft bake, place it on the hot plate with 90 ° C and 80 sec.

(4) Expose, contact the mask and the glass substrate by the aligner with filter for 150 sec.

(5) Developing, develop the PR with developer, FHD5, for 90 sec.

(6) Rinse, clean the substrate with DI water for 240 sec.

(7) After Develop Investigation (ADI), check the pattern with optical microscope.

(8) Hard bake, place on the hot plate with 120 ° C and 100 sec.
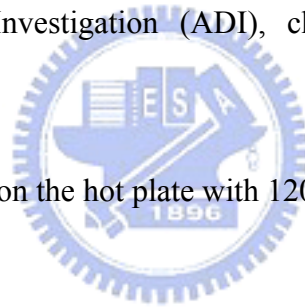
In order to etch the indium tin oxide (ITO) transparent layer on glass, an etchant have to be prepared with specific recipe of mixture. The adopted mixture is HCl : HNO_3 : H_2O = 1 : 0.08 : 1.

The detailed description of the wet etching procedures is provided as follow:

(1) Etchant preparation, prepare the etchant with the wet etching recipe: HCl : HNO_3 : H_2O = 1 : 0.08 : 1.

(2) Etching, put the sample in the prepared etchant, 2 min.

(3) Remove PR, put the sample in ultrasonic cleaner with ACE, 5 min.

(4) Dry, dry the glass with nitrogen gas blowing.

The detail processes of lithography and etching include initial cleaning, coating PR, UV exposure, develop, and chemical etching, as shown in Fig. 3-5.
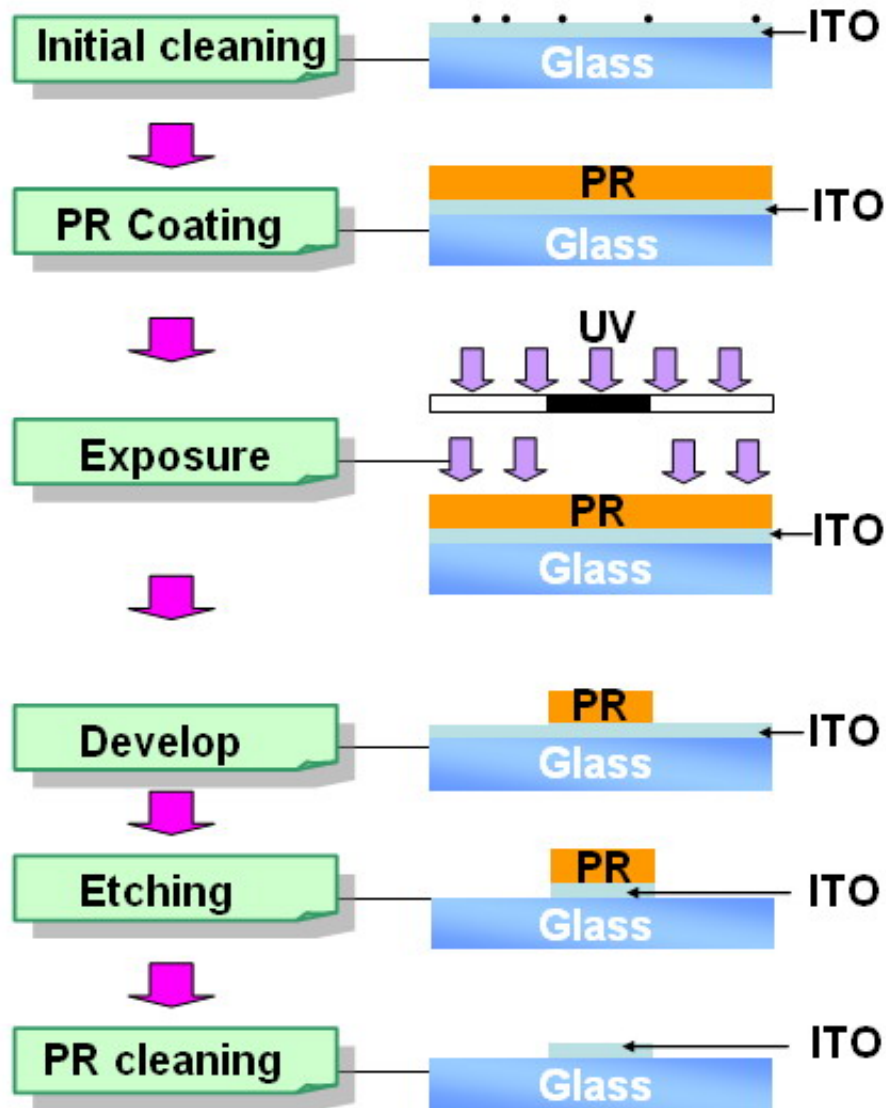

Fig. 3-5. Detail processes of lithography and etching to realize the technology of ITO electrode patterning

3.2.3 Metal electrode deposition and patterning

For the rear panel substrate, a conventional soda-lime glass was selected to be the substrate of the rear panel. The two reasons are proposed. Firstly, we only need the light transmit to the front direction of panel. Moreover, the metal electrodes fabricated by the sputtering deposition provide its reflectance to enhance the exploitation of the light emission. In addition, a lift off processes including sputtering and PR striping is used to pattern the metal electrode.

The initial surface cleaning and the photolithography processes have been completed with similar procedures described in previous sections. For the photolithography processes, HMDS layer is coated to improve adhesion. Usually a thick photoresist is used in lift-off process. Therefore, a uniform thick photoresist, AZ4620, is coated onto the soda-lime glass substrate and the parameters of AZ4620 are shown in Table 3-3. Exposure process is then implemented and the mask pattern is transferred onto the glass with photoresist, AZ4620. Next step, the exposed glass is immersed in the developer, AZ300, and the desired pattern will show up in the photoresist. The sputtering deposition by a six targets magnetic sputtering apparatus is then operated to deposit a metal layer after a desired pattern from the photolithography processes.

Sputtering is a physical process that atoms from a solid target material are ejected into the gas phase due to ion bombardment of the material by energetic ions. Sputtering is largely driven by momentum exchange between the ions and atoms in the material, due to collisions. The number of atoms from the surface per incident ion is called the sputter yield and is an important parameter of the efficiency of the sputtering process. Other things related to the sputter yield are the energy of the incident ions, the masses of the ions and target atoms, and the binding energy of

atoms in the solid. The ions for the sputtering process are supplied by plasma that is
ignited in the sputtering apparatus.

Table 3-3. Parameters of AZ4620 in the photolithography for lift-off.

AZ4620	
Type	Positive PR
Rotation speed and time	1st: 1000 rpm, 15 sec;
	2nd: 3500 rpm, 30 sec.
Soft bake	90 ° C, 510 sec
Exposure	490 sec.
Develop	180 sec
Rinse	240 sec
Thickness	8 μm
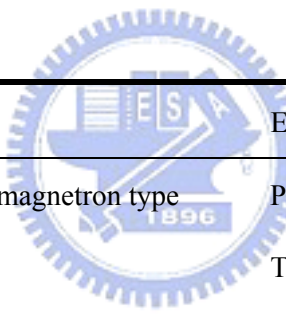
The detailed description of the photolithography procedures is provided as
follow:

(1) HMDS prime, coat a HMDS layer on surface and bake with 150° C in a

vacuum oven.

(2) Photoresist (PR) coating, place the substrate on a vacuum chuck in the

coater and drop appropriate PR on the center of the substrate: first step

with 1000 rpm, 15 sec and second step with 3500 rpm, 30 sec.

(3) Soft bake, place on the hot plate with 90 ℃, 510 sec.

(4) Expose, contact the mask and the glass substrate by the aligner with filter,

150 sec.

(5) Developing, develop the PR with developer, AZ300, 90 sec.

(6) Rinse, clean the substrate with DI water, 240 sec.

(7) After Develop Investigation (ADI), use the microscope to investigate the electrode pattern.

(8) Hard bake, place on the hot plate with 120 ° C, 100 sec.

Table 3-4 shows the specifications of six targets magnetic sputtering apparatus and the experimental parameters.

Table. 3-4. Specifications of sputtering system and experimental parameters.

Specifications		Experimental parameters	
Cathode	3" dia planar magnetron type	Process power	DC 0.1 kW
Total Power	DC 2KW	Thickness	1000 Å
Main pump	CTI Cryo pump 8	Time	615 sec
Base level	3.0×10^{-7} Torr	Deposition rate	1.62 Å/sec
Rotation	15 ~ 40 rpm		
Gas inlet	Ar, N2		

Deposition of the sputtered material tends to occur on all surfaces inside the vacuum chamber. Sputtering is used extensively in the VLSI semiconductor process to deposit thin films of various materials. Because of the low substrate temperatures used, sputtering is an ideal method deposit metals for display industry. Indium tin oxide (ITO) conducting coating layer on glass are also deposited by sputtering. Sputtering sources are usually magnetrons that utilize strong electric and magnetic fields to trap electrons close to the target surface of the magnetron. The electrons follow helical paths around the magnetic field lines undergoing more ionizing collisions with neutrals near the target surface. The typical sputter gas is argon, a kind of noble gases. The extra argon ions created from above collisions leads to a higher deposition rate. The sputtered atoms are neutrally charged and so are unaffected by the magnetic trap [21, 22]. Fig. 3-6 shows the schematic diagram of typical magnetic sputtering mechanism.
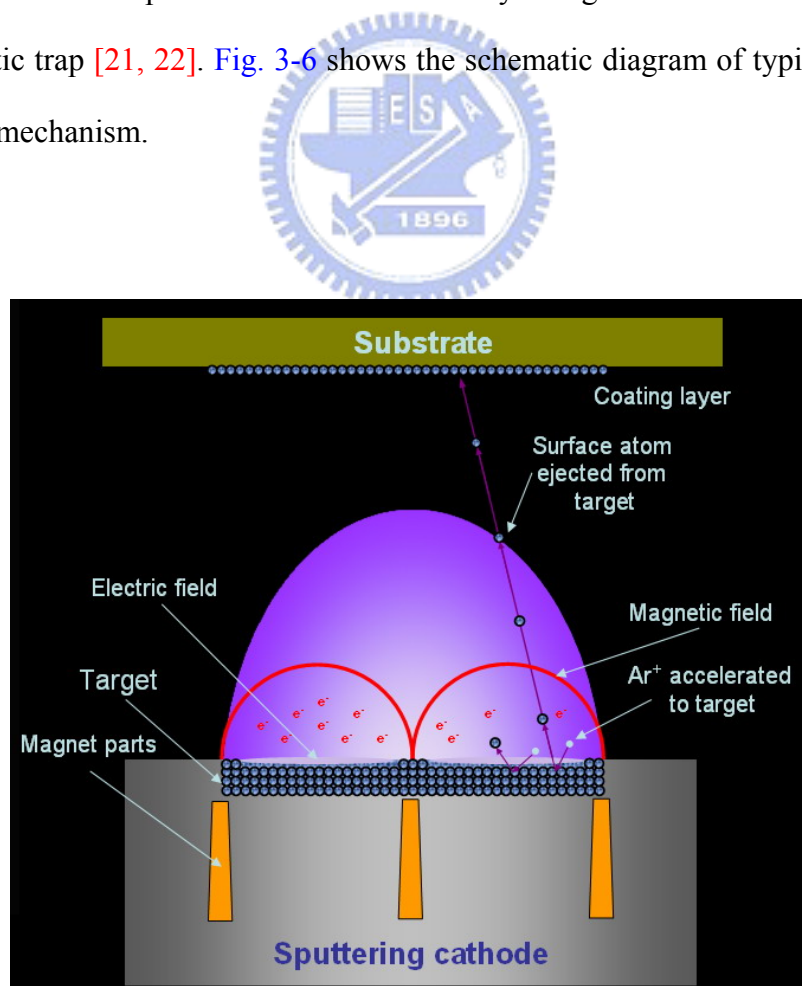

Fig. 3-6. Schematic diagram of magnetic sputtering mechanism.

Lift-off process is then used to define the desired pattern on the soda-lime glass substrate without etching after sputtering deposition. A desired pattern is fabricated on a substrate by the pattern of photoresist as described in last section. From sputtering process chromium (Cr) film is deposited all over the substrate, covering the defined photoresist pattern and non-photoresist areas. During the lift-off process, the photoresist under the Cr film is removed with organic solvent and the Cr film is taken off. Finally, the lift-off process leaves only the deposited Cr film with desired pattern on the glass substrate.

The detailed description of the metal electrode patterning including lift-off and sputtering processes is provided as follow:

(1) Chamber vent, put the substrate with desired pattern.

(2) Change the target to chromium target and check the electric contact between the chamber and the target.

(3) Chamber pump, achieve base vacuum level to 3.0×10^{-7} Torr and then inject the reactive gas, argon.

(4) Set the parameters of chromium deposition: DC 0.1 kW, 615 sec.

(5) Chamber vent, take out the sample with chromium film.

(6) Chamber pump, keep the vacuum state in the chamber.

(7) Lift-off, place the sample in ultrasonic cleaner with ACE.

(8) Rinse, put the sample in ultrasonic cleaner with DI water, 5 min.

(9) Dry, dry the glass with nitrogen gas blowing.

The detail processes of rear metal electrode patterning include initial cleaning, coating PR, UV exposure, develop, sputtering and lift-off, as shown in Fig. 3-7.
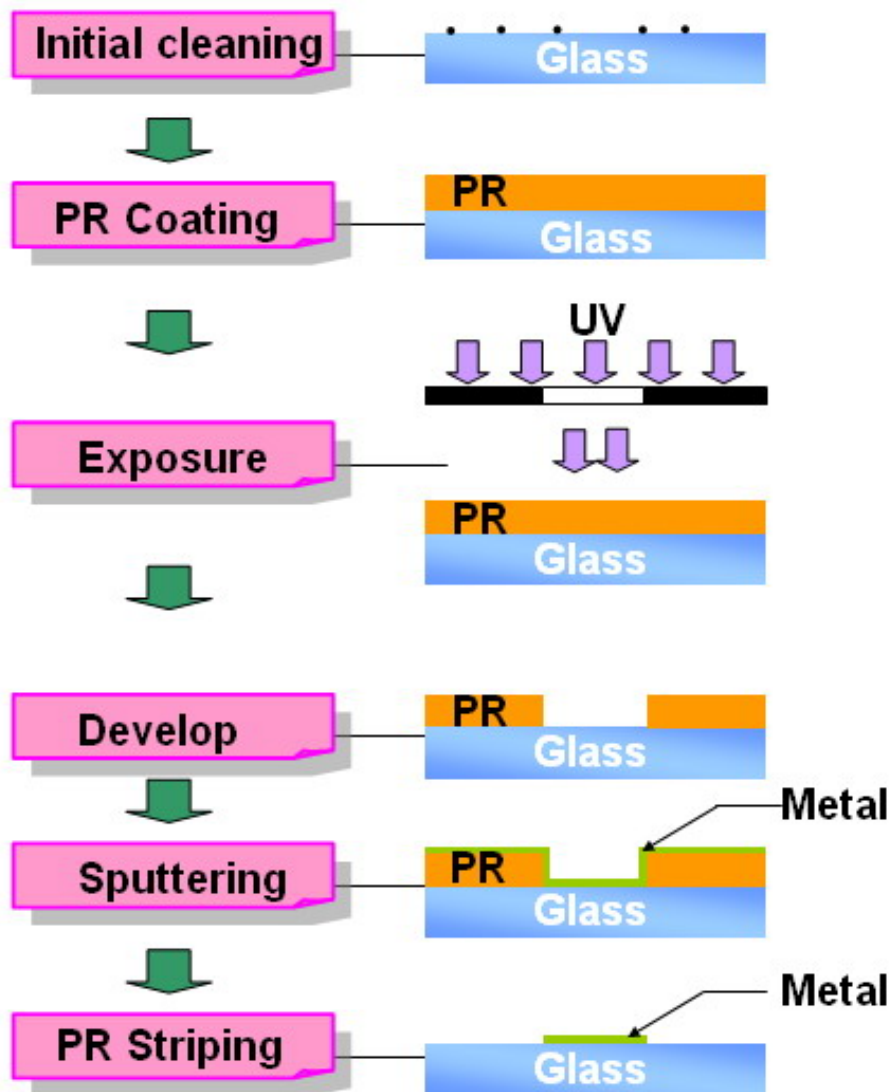
Fig. 3-7. Detail processes of photolithography, sputtering and lift-off to realize the technology of metal electrode patterning

3.2.4 Panel formation

The fabrication process to finalize a panel type microplasma device by glass substrate includes panel sealing with front and rear panels and sealing of exhausting tube. First we prepare the vacuum sealant by a given recipe A : B = 3 : 1. Vacuum sealant epoxy (Torr Seal, VARIAN) as shown in Fig. 3-8 is a solvent-free sealant for high vacuum application and it can suffer vacuum level lower to 10^{-9} Torr, and temperatures from –45° C to 120° C. In addition, it is suitable for many materials including metal, ceramic, and glass. Gap distance between electrodes is guaranteed by specific spacers, thin soda-lime glass with a thickness of 400 μm. The panel sealing process is one that the vacuum sealant is applied on the edges of rear substrate and the front substrate is then covered on it. The pre-sealed panel is placed on the hot plate with temperature curing for 8 hours. Next step, the exhausting tube is connected to the exhausting hole on rear substrate by a same process. The above mentioned process is similar with that in plasma display panel (PDP) industry.

Fig. 3-8. Photograph of Torr seal for panel sealing.

3.3 Very High Vacuum (VHV) System

3.3.1 Vacuum technology

"Vacuum" is a space from that air or other gas has been removed. In practice, all the gas can never be removed and air is the most important gas to be pumped because it is in every system. The usual pressure unit is shown as follow.

$$1 \text{ atm (standard atmosphere)} = 760 \text{ mm-Hg} = 760 \text{ torr} = 1013 \text{ mbar}$$

$$= 1.013 \times 10^5 \text{ Pa (Pascal)} = 14.7 \text{ psi}$$

$$= 1.03327 \text{ kg/cm}^2$$

For convenience it is customary to divide the pressure scale blow atmospheric into several ranges and to relate phenomena and processes to them. Table. 3-5 lists the vacuum degree range. Epitaxial growth of semiconductor films takes place in the low vacuum in low vacuum range. Sputtering plasma etching and low pressure chemical vapor deposition are performed in the medium vacuum range. Pressures in the very high vacuum are necessary for thin-film preparation, mass spectroscopy, crystal growth, electron microscopy, and the production of cathode ray tube. Pressure in ultra high range is required got material and surface research work [23].

The degree of vacuum state can affect the physical characteristics. Mean free path and gas molecular density are important factors in vacuum. Higher vacuum degree causes lower number of gas molecules in space and the influence in experiment from gas molecules is smaller [24].

Degree	Pressure range	Molecule number	Mean free path	Pump type
	Torr	cm^{-3} (at $20\,^{\circ}C$)	cm	
Low	760 - 100	$2.5\times10^{19} \sim 3.3\times10^{18}$	$5\times10^{-6} \sim 5\times10^{-5}$	Mechanical pump
Medium	100 - 1	$3.3\times10^{18} \sim 3.3\times10^{16}$	$5\times10^{-5} \sim 5\times10^{-3}$	Combination of Mechanical pump and diffusion pump
High	1 - 10^{-4}	$3.3\times10^{16} \sim 3.3\times10^{13}$	$5\times10^{-3} \sim 5$	
Very high	10^{-4} - 10^{-8}	$3.3\times10^{13} \sim 3.3\times10^{9}$	$5 \sim 5\times10^{4}$	Combination from Mechanical pump, diffusion pump, Ion pump, Turbo pump, Cryo pump and Titanium sublimation pump
Ultra high	$\leq 10^{-9}$	$\leq 3.3\times10^{8}$	$\geq 5\times10^{4}$	

3.3.2 Vacuum equipment

Material of vacuum parts, selection and disposal of pump and installation of each part are important factors to make good vacuum environment. One of the most troublesome issues in vacuum state is gas release from solid materials at low pressure. There is the slow evolution of additional gases and vapors from the interior surfaces to prolong the pumping time. The surface gas release result from several potential processes including vaporization, thermal desorption, diffusion, permeation, and electron- and ion-stimulated desorption. Fig. 3-9 shows all potential sources of gases in a vacuum system [21].
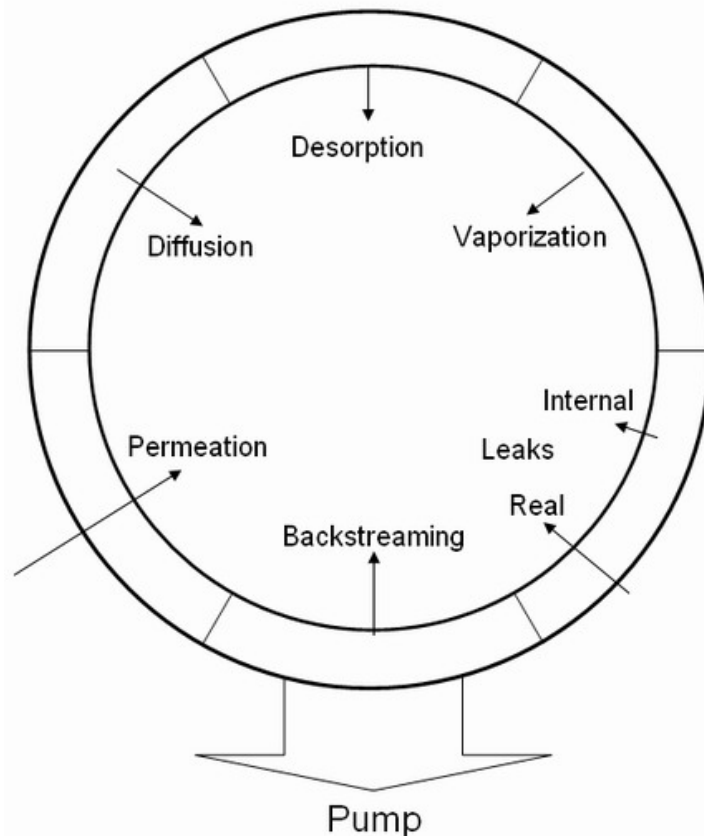
Fig. 3-9. Potential sources of gases and vapors in a vacuum system.

Gas diffusion from the wall of vacuum container contributes to the outgassing of the system and it is formed by the thermal motion of atoms or molecules. Permeation is a three steps process including adsorbing, diffusion, and desorbing and it depends on temperature and pressure. A vapor is a gas near its condensation temperature and vaporization is thermally stimulated entry of molecules into the vapor state. Vapor pressure is caused by the pressure of vaporization at specific temperature, and vapor pressure changes with different temperature and materials. A vacuum system consists of many sub-systems and parts. Sub-systems comprise chamber, vacuum gauge, vacuum pump and etc. are assembled with flange, O-ring, gasket, trap, feedthrough, valves and other elements. Leaks can be divided into real leak and virtual leak. A real leak is one that is coming into the vacuum chamber from an outside source. A virtual leak means a gas load evolving from inside the vacuum system from outgassing.

44

Correct vacuum sealing mechanism and suitable sealing components or materials can make the desired vacuum environment. In general, there are two seal methods between flanges, which are O-ring type and oxygen-free high conductivity copper (OFHC) gasket type. The O-ring type is only suitable for medium vacuum level and the material is elastic polymer. When the excepted vacuum level is less then 10^{-7} Torr or the temperature is more than 200 $^\circ$C, OFHC gasket type is used for better airtightness.

3.3.3 Setup of very high vacuum system

To have high purity gas content in our microplasma device, a very high vacuum environment is essential. The base level of the very high vacuum system in our laboratory is about 10^{-7} Torr. In order to achieve and maintain the base level, two mechanical rotation pumps and a turbo molecular pump have been selected.

Turbo molecular pump is using high rotation speed turbo vanes (50,000 rpm, pumping speed for N_2 is 145 l/sec). The advantages of turbomolecular pump are the pumping speed is high and there is no oil contamination like the diffusion pump. However, turbo pump is using the high rotation speed turbo vanes, and it may cause vibration issue. Some experiments which need a non-vibration environment are not suitable for turbo molecular pump such as scanning tunneling microscope (STM) and atomic force microscope (AFM). In a turbomolecular pumped system, a forepump with sufficient capacity should be chosen to keep the vane nearest the foreline in molecular flow or just in transition flow at maximum speed.

Two mechanical pumps are used in our very high vacuum (VHV) system. First one is the forepump for the vacuum chamber and the second one is the forepump for the turbomolecular pump. When the first forepump speed be large enough to keep the rough chamber pressure below the critical pressure and the turbomolecular pump is then turned on to achieve research base vacuum level. The second forepump is responsible for the rough pressure of turbomolecular pump which is separated

The detailed description of the VHV system operating procedures is provided as follow:

(1) Turn off high vacuum gauge, close the manual gate valve between turbo pump and chamber, and turn off power of all pumps.

(2) Purge with He gas, open the main window and clean

(3) Turn on two mechanical pumps, check the reading value of vacuum baratron gauge.

(4) While achieve $10^{-2} \sim 10^{-3}$ Torr, turn on the turbo molecule pump.

(5) While turbo pump get full speed, close the inline valve between the chamber and the foreline mechanical pump of chamber. Open the gate valve between turbo pump and chamber; turn on the high vacuum gauge.

(6) Gas filling: while the reading value of the high vacuum gauge achieve base pressure 10^{-7} Torr and close the gate valve between turbo pump and chamber. Inject research gas and adjust pressure with needle valve.

(7) Turn off the turbo pump, after 30 min. turn off mechanical pumps.

The nano-tip enhanced microplasma device was connected to the very high vacuum system with an adapter fitting (Ultra torr, Swagelok). Different gases or gas mixtures are injected into the vacuum system and the research pressure is adjusted with a needle valve and measured by a baratron gauge (628B, MKS). A photograph of the very high vacuum system is presented in Fig. 3-10.
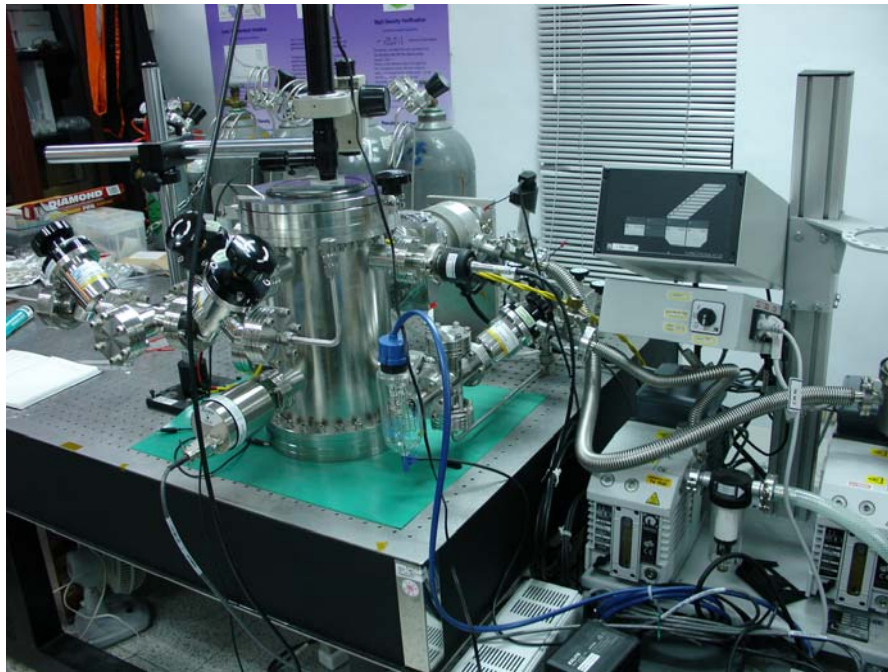
Fig. 3-10. Photograph of designed VHV vacuum system.

3.4 Measurement Instruments

Discharges are excited by bipolar pulsed signal, an electric pulsed power source set including a pulse power controller (SHENCHANG ELECTRIC, SPIK 2000A; 0-1 kV, 2 kW) and a direct current power supply was used to input the waveform. The DC power supply provides the energy to pulse power controller and output the pulse power. The bipolar pulsed excitation waveform, having the duty ratio with 20%, was applied with the frequency from 2 to 20 kHz between the front ITO electrode and the rear metal electrode by the pulsed power source. The discharge current and voltage were measured by a 1 kΩ resistor in series and a voltage probe in parallel, respectively. The photograph of the electric pulsed power source set is shown as Fig. 3-11.

Fig. 3-11. Photograph of pulsed power source set.

An image observation system including a color charged-coupled device (CCD) camera (Watec, WAT-202D), a zoom lens set (NAVITAR, Zoom 6000), a digital

camera, and a personal computer, is used to record the discharge phenomenon. The light emitted from the glow discharge was recorded using a color charged-coupled device (CCD) camera. With a zoom lens set, the discharge was imaged on the personal computer by a capture card. When a large-scale discharge area was needed, a digital camera was utilized to record the optical appearance of the glow discharge.

Chapter 4

Results and Discussion

4.1 Introduction

In this chapter, the experimental results including electrical properties and optical appearances of nano-tip enhanced microplasma devices will be presented. The main idea for adopting nano-tip in the microplasma is to locally enhance the electric field when a potential difference is applied on the electrodes. While the external electrical field exceeds a threshold value, a gas discharge is ignited. Enhanced electrical field in proposed devices provide higher probability to achieve gas breakdown phenomenon at lower operating voltage.

The collected data of electrical properties including current-voltage (I-V) characteristic, voltage margin and memory coefficient from discharges operating in neon, argon and Ne+Ar(2%) as filling gases are presented and discussed. First, the current-voltage characteristic reveals the positive differential resistance, one signature of the abnormal glow discharge, over entire operating pressure. Secondary, operating voltage properties and voltage margin are introduced and discussed. Next, the memory coefficient is given to compare the probability of stable discharge phenomena in neon, argon and Ne+Ar(2%). Furthermore, optical appearance containing charged-coupled device (CCD) images of discharge and photographs of operated devices will be presented at the end of this chapter.

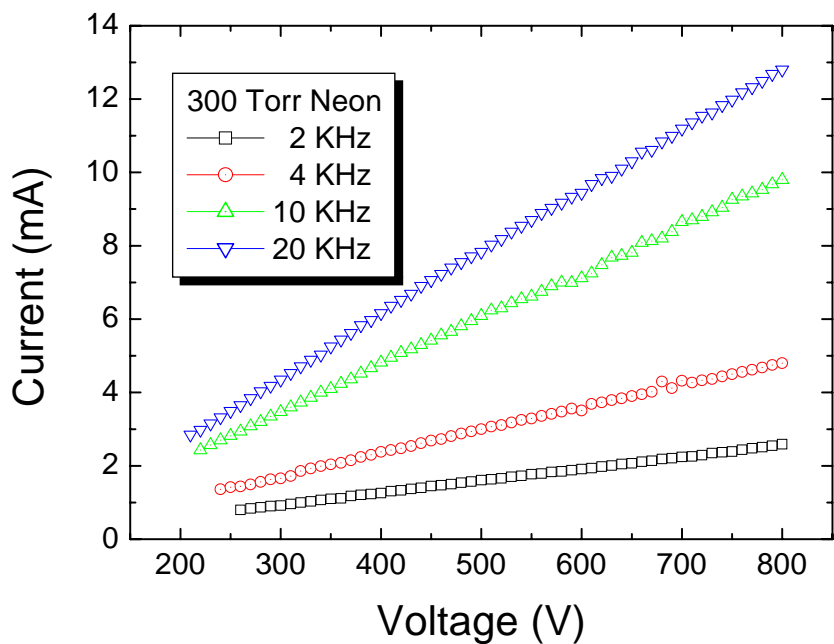## 4.2 Current-voltage (I-V) characteristics

The breakdown can be defined as the transformation of a non-conductive medium into a conductive medium, when a sufficiently strong electrical field is applied. The current-voltage (I-V) characteristics of a discharge in the nano-tip enhanced microplasma devices can provide valuable information about the mechanism as described for the case of glow discharge in Section 2.2.

The specification of bipolar pulsed excitation signal which was applied to ignite the discharge was shown in Table 4-1. The applied signal was provided from an electric pulsed power source set. The amplitude of applied voltage is adjustable from 0 to 1000 V and the excitation frequencies are selected with 2, 4, 10 and 20 kHz. To acquire current-voltage (I-V) characteristics, the discharge was ignited by a potential about 250 V with the electric pulsed power source set. The discharge current and voltage were measured by an external resistor in series and a voltage probe in parallel, respectively.

Table. 4-1. Parameters of bipolar pulsed excitation signal.

Parameter	Condition
Waveform	Pulse
Frequency	2, 4, 10 and 20 kHz
Amplitude	0-1000 V (Peak)

The current-voltage (I-V) characteristics for the nano-tip enhanced microplasma devices are operated in 300 and 400 Torr of neon gas as shown in Fig. 4-1 for various value of V where the slope of the current-voltage characteristic is positive.
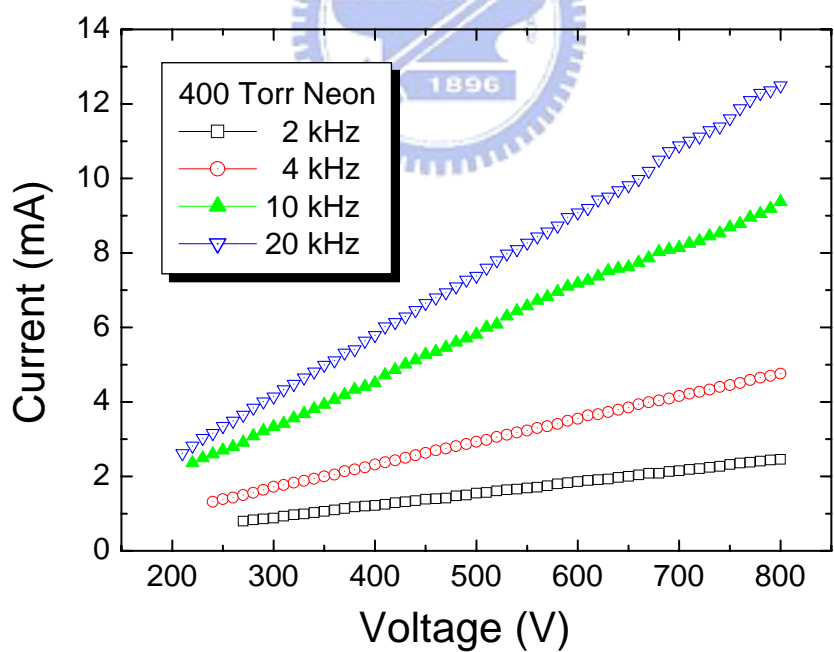
Fig. 4-1. Current-voltage characteristics of the devices operated in neon and excited by a bipolar pulsed waveform of 2, 4, 10, or 20 kHz: (a) 300 Torr, (b) 400 Torr.

In Fig. 4-1, the current-voltage (I-V) traces of the microplasma devices with direct current bipolar pulsed excitation frequencies of 2, 4, 10 and 20 kHz are characterized by a positive effective plasma resistance, one signature of the abnormal glow discharge mode, over all of the operating ranges for neon gas at room temperature. In the abnormal glow discharge mode, the current is increased by increasing the voltage to supply more electrons to the discharge. The current-voltage traces reveal linear relationship between operating voltage and discharge current. Therefore, the power consumption can be predicted by this linear relationship. While the excitation frequency is increased, the sustaining voltage is found to decrease from approximately 270 V at 2 kHz to 215 V at 20 kHz. The effective plasma resistance, R_{eff}, can be estimated at the various excitation frequencies by calculating the slope of the I-V curves. The reproducibility of these measurements is such that each of these curves is reproducible to within 0.5 mA and they exhibit a positive effective plasma resistance, R_{eff}, between 58 kΩ (2 kHz) and 317 kΩ (20 kHz). From the result, as the excitation frequency is increased, the discharge becomes more conductive. Regardless of the driving frequency in the range, the devices are operated in the abnormal glow mode and the plasma effective resistance falls by more than a factor of five while the excitation waveform periodicity is decreased from 500 μs (2 kHz) to 50 μs (20 kHz). While the excitation frequency was 20 kHz, currents of 2.8 to 12.8 mA were recorded for pulsed voltages of 210 to 800 V at 300 Torr, and currents of 2.6 to 12.5 mA were recorded for pulsed voltages of 220 to 800 V at 400 Torr. Moreover, the I–V characteristics are very similar over the entire range of gas pressures (300 – 800 Torr) under neon, argon and Ne+Ar(2%).

4.3 Operating voltage

In this section, the firing voltage and minimum sustain voltage of the proposed microplasma device will be investigated as the parameter of operating voltage. The firing voltage (V_f) is the voltage amplitude which changes the state of the device from nondischarge (OFF) to discharge (ON), and the minimum sustain voltage is the minimum voltage amplitude which sustains a discharge sequence. A sustain voltage supports the sequence of electric discharges, but it can not initiate a discharge sequence. Any voltage amplitude above V_f will initiate a discharge sequence, and any voltage amplitude below V_{sm} will be inadequate to sustain a discharge sequence. Electrical properties of operating voltage were investigated as a function of the following parameters: bipolar pulsed excitation frequency, operating pressure and gas content in our experiment.

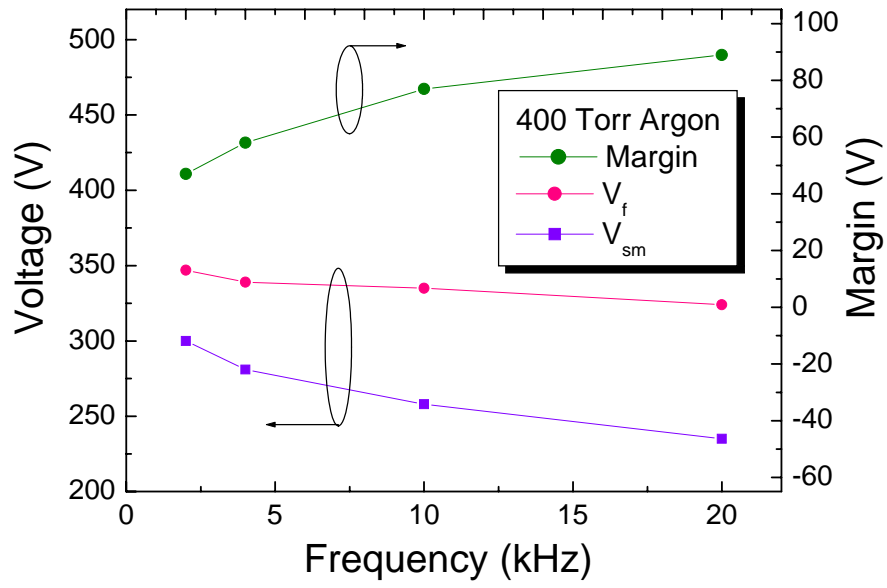### 4.3.1 Excitation frequency

The voltage margins of the firing voltage (V_f) and the minimum sustain voltage (V_{sm}) for the devices on different excitation frequencies from 2 to 20 kHz for neon, argon, Ne+Ar(2%) at pressures of 400 Torr and 500 Torr is illustrated in Fig. 4-2. The results show that the higher the oscillating frequency, the larger the voltage margin was. A voltage margin is defined by the voltage difference between a firing voltage and a sustain voltage. A stable discharge phenomenon can be acquired in the range of voltage margin. Moreover, with the addition of argon gas in neon gas, the operating voltages were improved. The results in neon, argon, Ne+Ar(2%) mean that high frequencies are adequate to drive the devices at low driving voltages with large voltage margin. Furthermore, in all gases used here the voltage margin of the microplasma was found to be similar over the entire range of gas pressures.
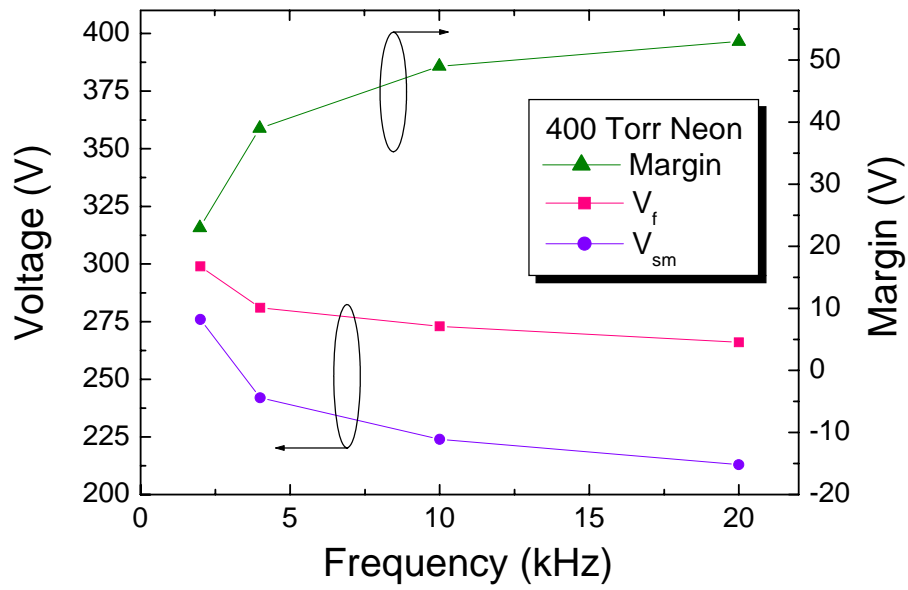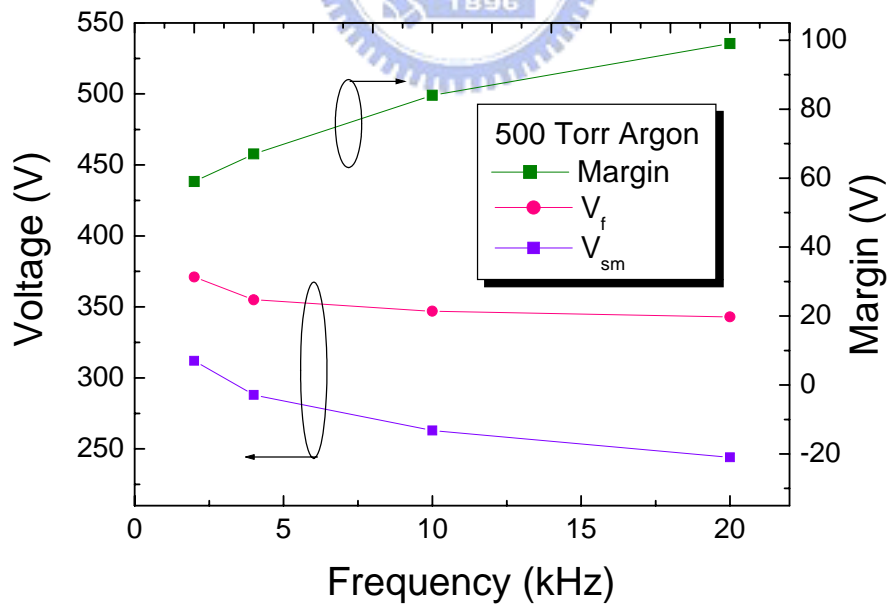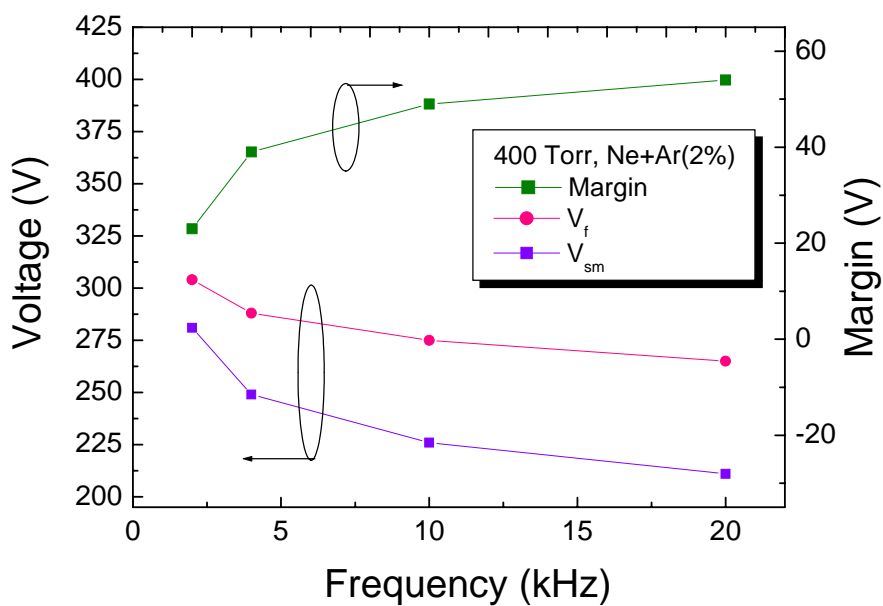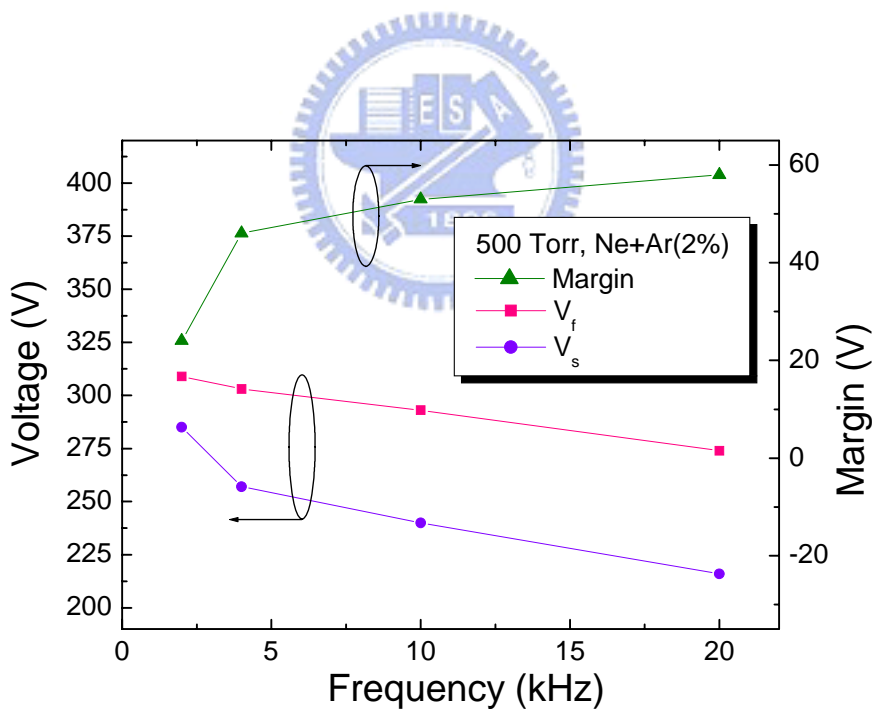
(a)
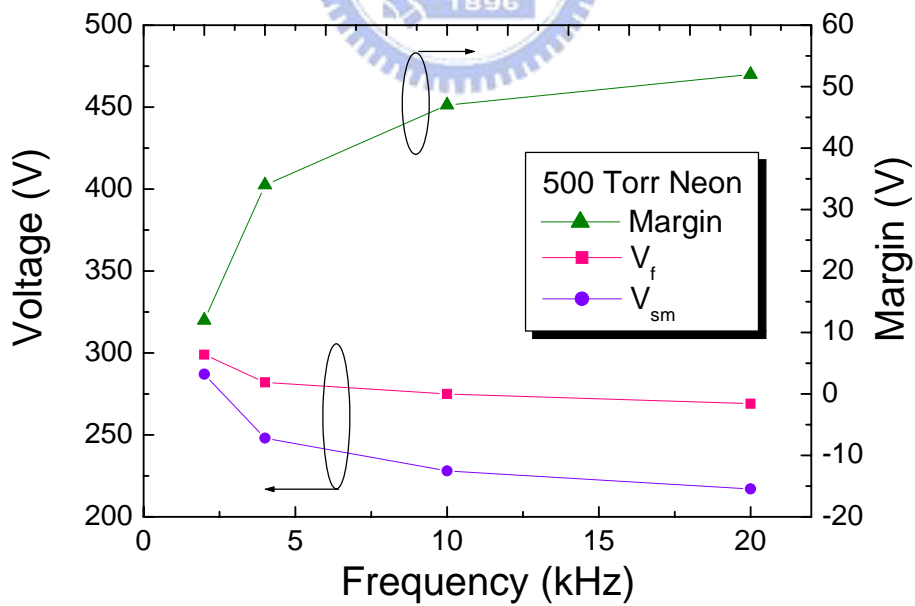
(b)

(c)

(d)

(e)

(f)

Fig. 4-2. The margin of firing voltage (V_f) and minimum sustain voltage (V_{sm}) for the devices on different excitation frequencies of 2, 4, 10, and 20 kHz: (a) neon, 400 Torr, (b) neon, 500 Torr, (c) argon, 400 Torr, (d) argon, 500 Torr, (e) Ne+Ar(2%), 400 Torr, (f) Ne+Ar(2%), 500 Torr

57

4.3.2 Operating pressure

Fig. 4-3 illustrates the relationship between the operating pressure and discharge voltage including firing voltage (V_f), minimum sustain voltage (V_{sm}) and an average parameter, V_o, of the devices on different excitation driving frequencies of 2, 4, 10, or 20 kHz for a neon gas at pressures between 300 Torr and 800 Torr. When the value of operating voltage achieve firing voltage (V_f) amplitude, the state of the microplasma device from nondischarge (OFF) to discharge (ON). Because of the self-sustained discharge phenomenon, a minimum sustain voltage (V_{sm}) amplitude which is lower the value of firing voltage (V_f) can be obtained. For convenient, V_o is introduced to observe the variation of the operating voltage with different gas pressures. In the figure, the operating voltage, V_o can be determined as an average parameter of the firing voltage (V_f) and the minimum sustain voltage (V_{sm}) as shown in Equation (4.1).
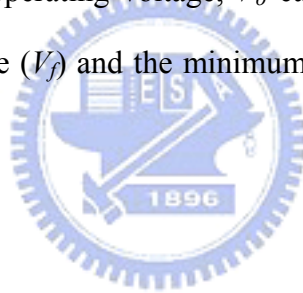
$$V_o = \frac{1}{2}(V_f + V_{sm}) \tag{4.1}$$

It can be noticed from the results the firing voltage and the minimum sustain voltage could be reduced by decreasing the operating pressure due to the increased mean free path of the energetic particles. The mean free path is defined as the average distance that an object can move before colliding with another particle. Therefore, the higher colliding frequency is, the lower mean free path will be. Under the same electrical field, the mean free path is inversely proportional to the colliding frequency. The relationship between the mean free path and the highest energy of an electron is calculated as follows,

$$W_e = F \times d = q \cdot E \cdot \lambda \tag{4.2}$$

where W_e is the energy of an electron, F is the force, d is the distance, q is the quantity of electricity, E is the electric field, λ is the mean free path

From Equation (4.2), the energy from the accumulated work of electrons by the electric field increases with the electric field or the mean free path. Accordingly, high voltages and low pressures are generally suitable for the plasma operation. As the gas pressure drops, the mean free path of the gas increases and the kinetic energy of the electrons will also increase, meaning that a collision with a gas molecule will be more likely to result in ionization. Beside, with the electrode gap and operating pressure and the *pd* values are from 12 to 32 cm-Torr, the relationship between operating pressure and discharge voltage is match with *Paschen Curve*. In accordance with above reasons, therefore, the firing voltage is decreased with the decrease in the gas pressure.
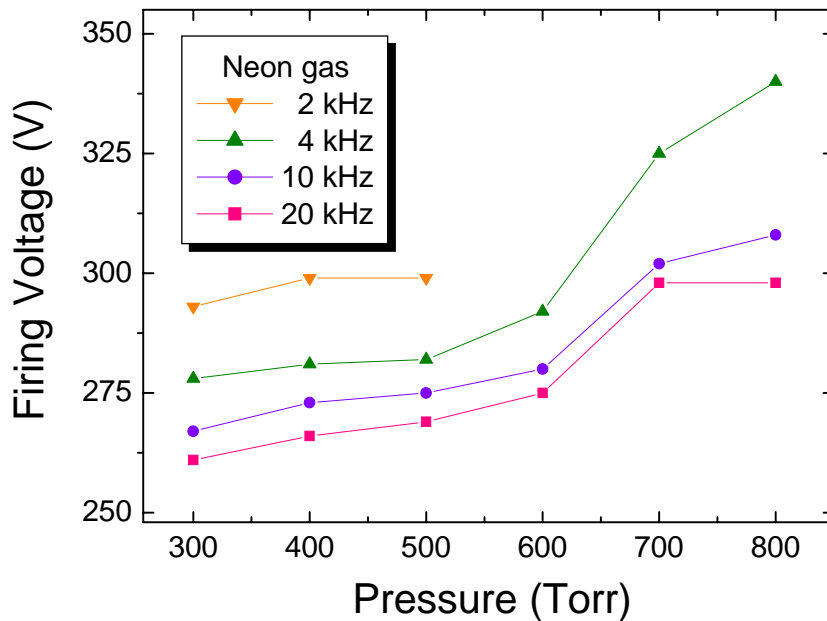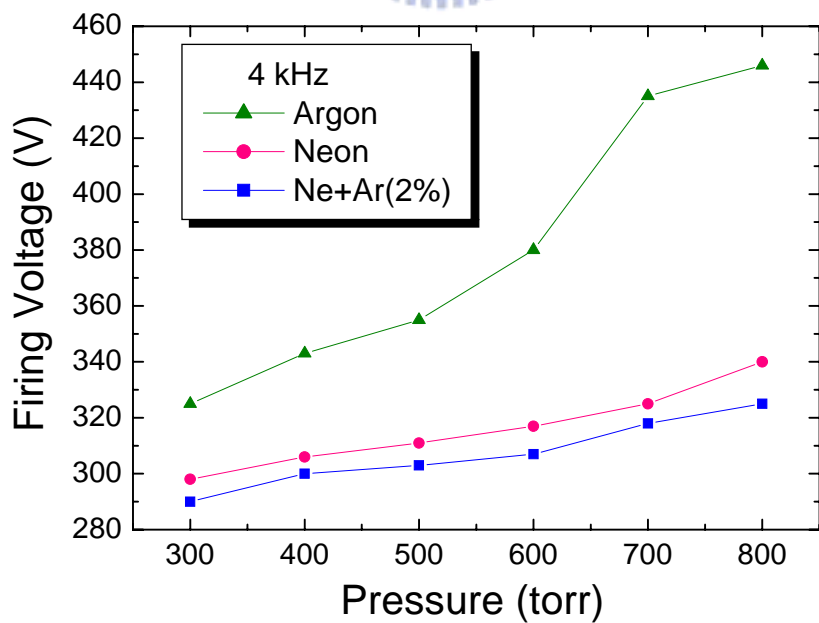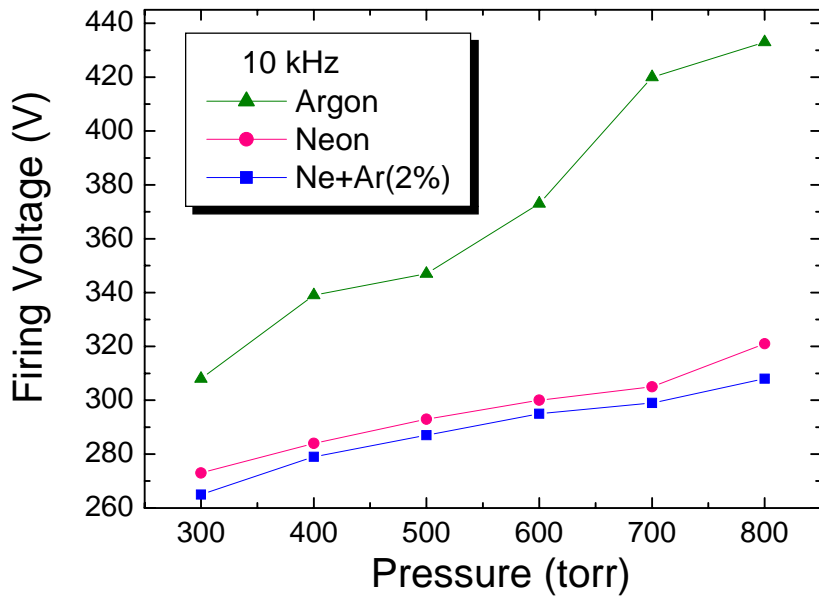

(a)
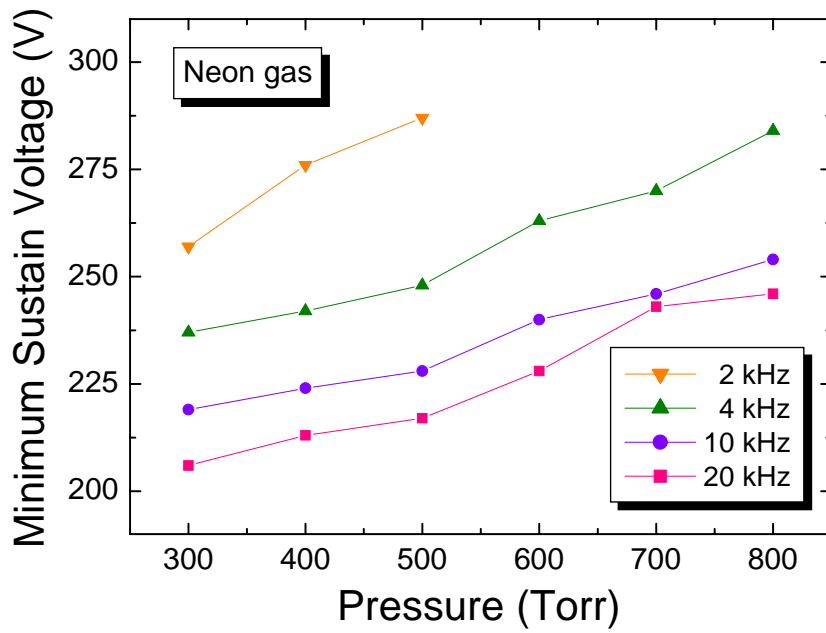
(b)
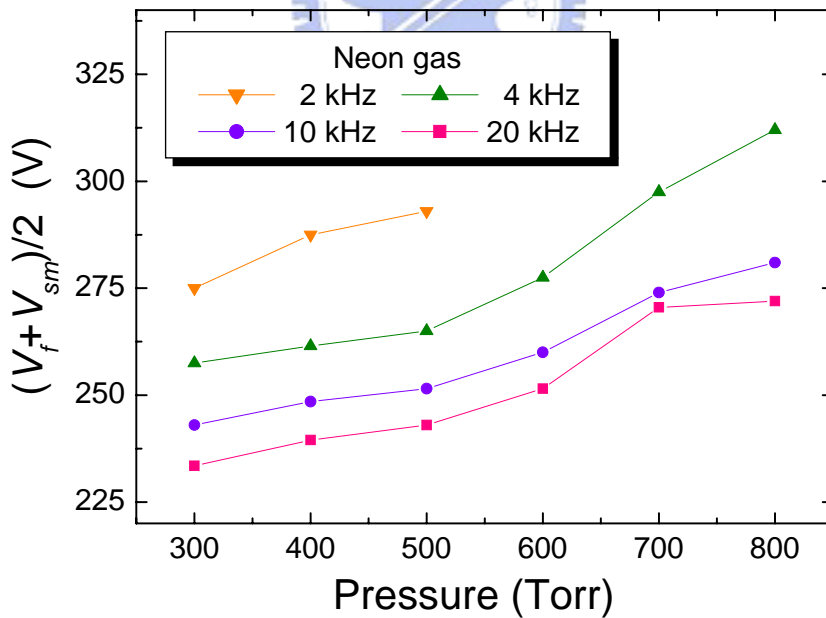
(c)

Fig. 4-3. The relationship between the discharge voltage and operating pressure of the devices on different excitation frequency 2, 4, 10, or 20 kHz for a neon gas pressure from 300 Torr to 800 Torr: (a) firing voltage (V_f), (b) minimum sustain voltage (V_{sm}), (c) $V_o=(V_f+V_{sm})/2$.

4.3.3 Gases content

Fig. 4-4 shows the firing voltage measurement as a function of operating pressure and gas content on various direct current bipolar pulsed excitation waveforms frequencies. As shown in Fig. 4-4, the firing voltage varies substantially with the various gas contents. The voltage difference between neon and argon are 40 to 140 V at gas pressures from 300 Torr to 800 Torr. With the addition of argon in pure neon, the firing voltage is reduced about 10 V at whole gas pressure range. At Ne+Ar(2%) gas pressure of 300 Torr, the firing voltage decreases from 261 V in pure neon to 250 V with a direct current bipolar excitation frequency of 20 kHz. A *Penning effect* which provides a lower igniting voltage plays the role in this phenomenon. A *Penning gas mixture* consists of an inert gas containing another gas which has lower ionization potential than or equal to the metastable potential of the origin inert gas.


(a)

(b)
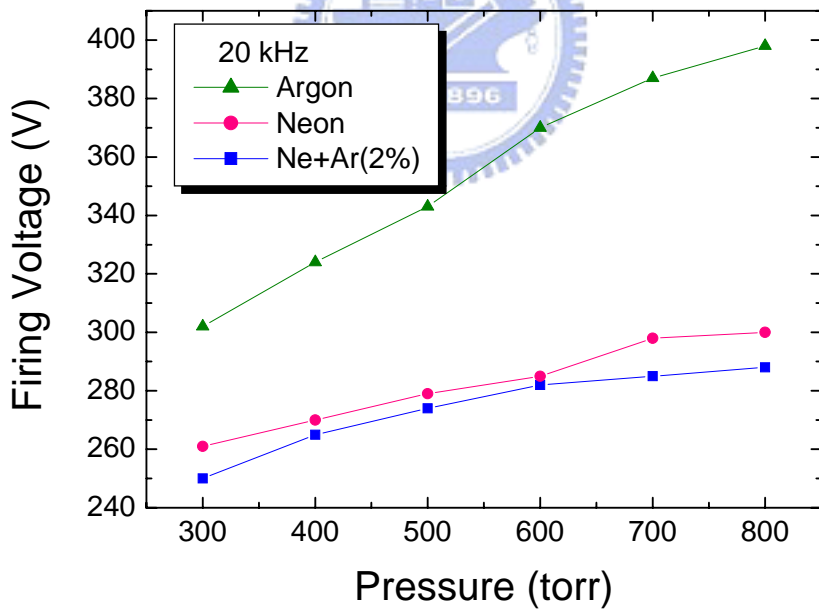
(c)

Fig. 4-4. The relationships between the firing voltage and operating pressure of the devices on different gas content at gas pressures from 300 to 800 Torr on various excitation frequencies of (a) 4 kHz, (b) 10 kHz, and (c) 20 kHz.
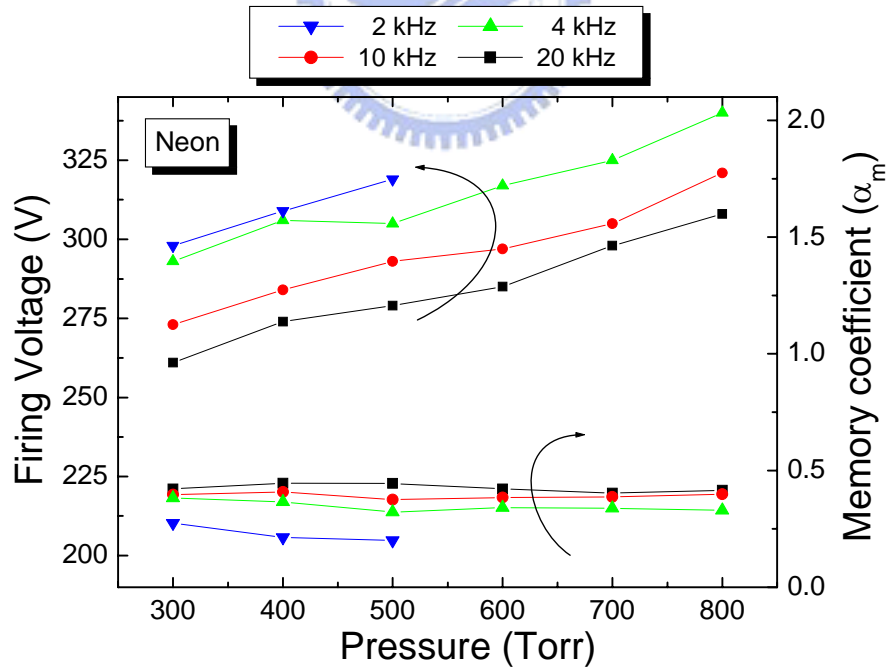
4.4 Memory coefficient

Fig. 4-5 illustrates the dependence of memory coefficient (α_m) and firing voltage (V_f) on the operating pressure from 300 Torr to 800 Torr with different pulsed excitation frequencies at 2, 4, 10, and 20 kHz. Memory coefficient is widely used to estimate the margin performance of plasma display panel (PDP). The definition of memory coefficient (α_m) derived from the quality of voltage margin is shown by the following equation [25-27]:

$$\alpha_m = \frac{(V_f - V_{sm})}{V_f / 2} \tag{4.2}$$

The memory coefficient (α_m) is related to the stability that is to sustain a discharge at a voltage lower than that required for initiating it. When the memory coefficient (α_m) value is large, the higher probability of stable discharge phenomena is acquired. Regardless of gas content, the voltage required to ignite a discharge decreases significantly with the increase of excitation frequency. In addition, higher memory coefficient (α_m) is obtained with excitation frequency on 20 kHz, and the similar calculated results are acquired in neon, argon and Ne+Ar(2%). On the contrary, with excitation frequency on 2 kHz, lower memory coefficient (α_m) is obtained and the glow discharge phenomenon is too weak to sustain. Consequently, with a relatively high excitation frequency, a low firing voltage can be acquired and an intense glow discharge phenomenon can be found stably.

(a)

(b)

64
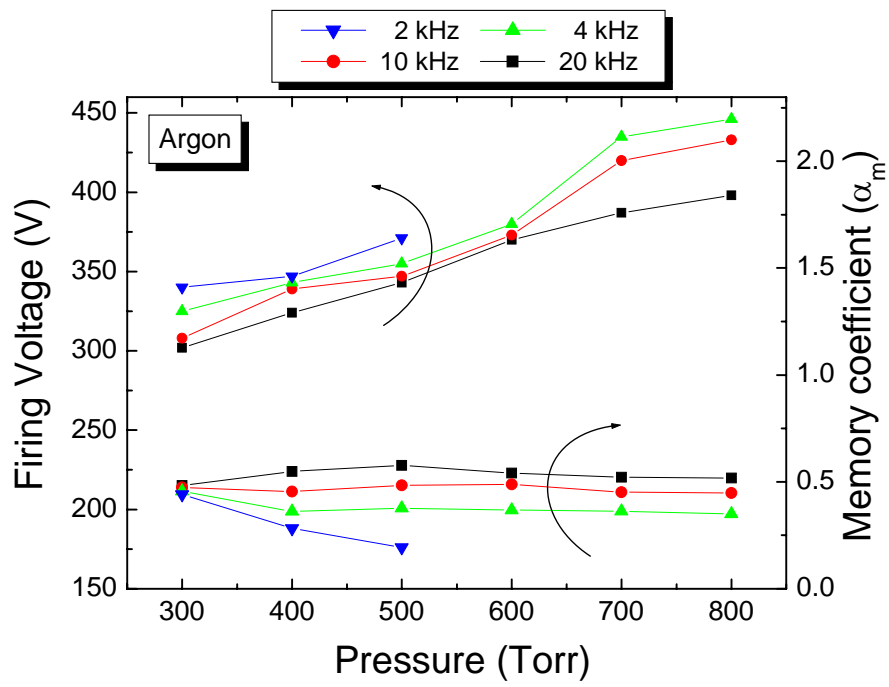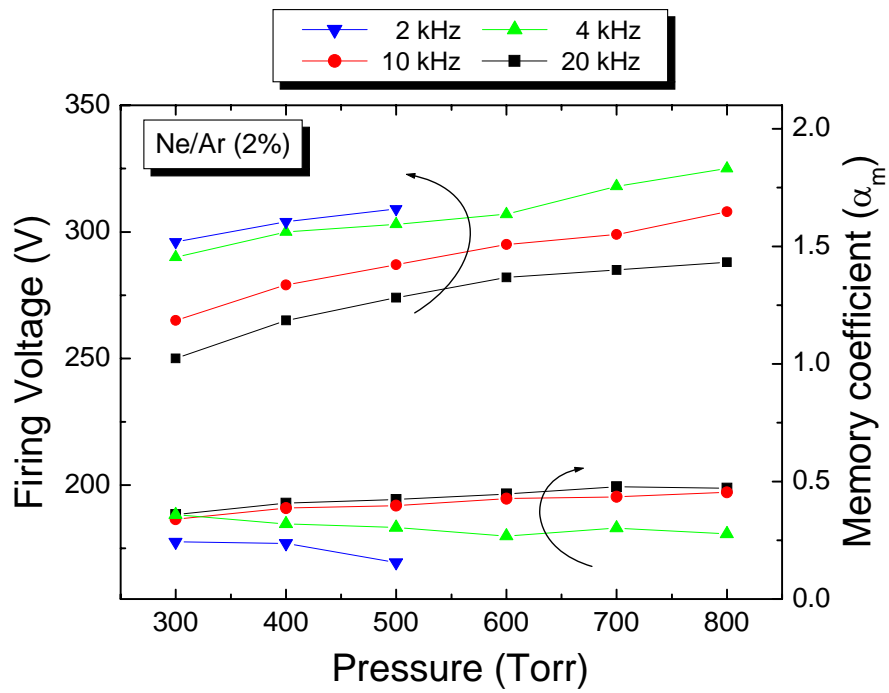
Fig. 4-5. Dependence of the firing voltage and memory coefficient (α_m) on working pressures of the devices with different excitation frequencies of 2, 4, 10, and 20 kHz: (a) neon, (b) argon, (c) Ne+Ar(2%).

4.5 Optical appearance

Fig. 4-6 exhibits the discharge charged-coupled device (CCD) images of the operated nano-tip enhanced microplasma devices at 400 Torr of neon gas with varying bipolar pulsed excitation and frequencies of 4, 10, and 20 kHz. The images are captured by an image observation system including a color charged-coupled device (CCD) camera (Watec, WAT-202D), a zoom lens set (NAVITAR, Zoom 6000), a digital camera, and a personal computer. The operating voltages of the discharge CCD images are 300 V and 600 V in Fig. 4-6. With higher excitation frequency and applied voltage, the optical appearance of the discharge changes from relatively dark to bright and the light emission also become more intensive.

In addition, the standing *striation* phenomena from the metal electrode edge are observed from the CCD images. The *striation* means the traveling waves or stationary perturbations in the electron number density which occurs in partially ionized gases. *Striation* is known in positive column and ionospheric plasma system, and it is related to the wave mechanism. *Striation* in typical dielectric microdischarge device is basically governed by the ionization-dominated α-process.

Fig. 4-7 presents photographs of the entire operated nano-tip enhanced microplasma devices operating with neon, argon and Ne+Ar(2%). The gas pressure and excitation frequency were fixed at 400 Torr and 20 kHz. Because there is only a dielectric with ITO electrode and dielectric can provide wall charge effect, the discharge expands with the pattern of ITO transparent electrode. High intensity of glow discharge in proposed devices reveals its potential of extended development in future work.

(a)
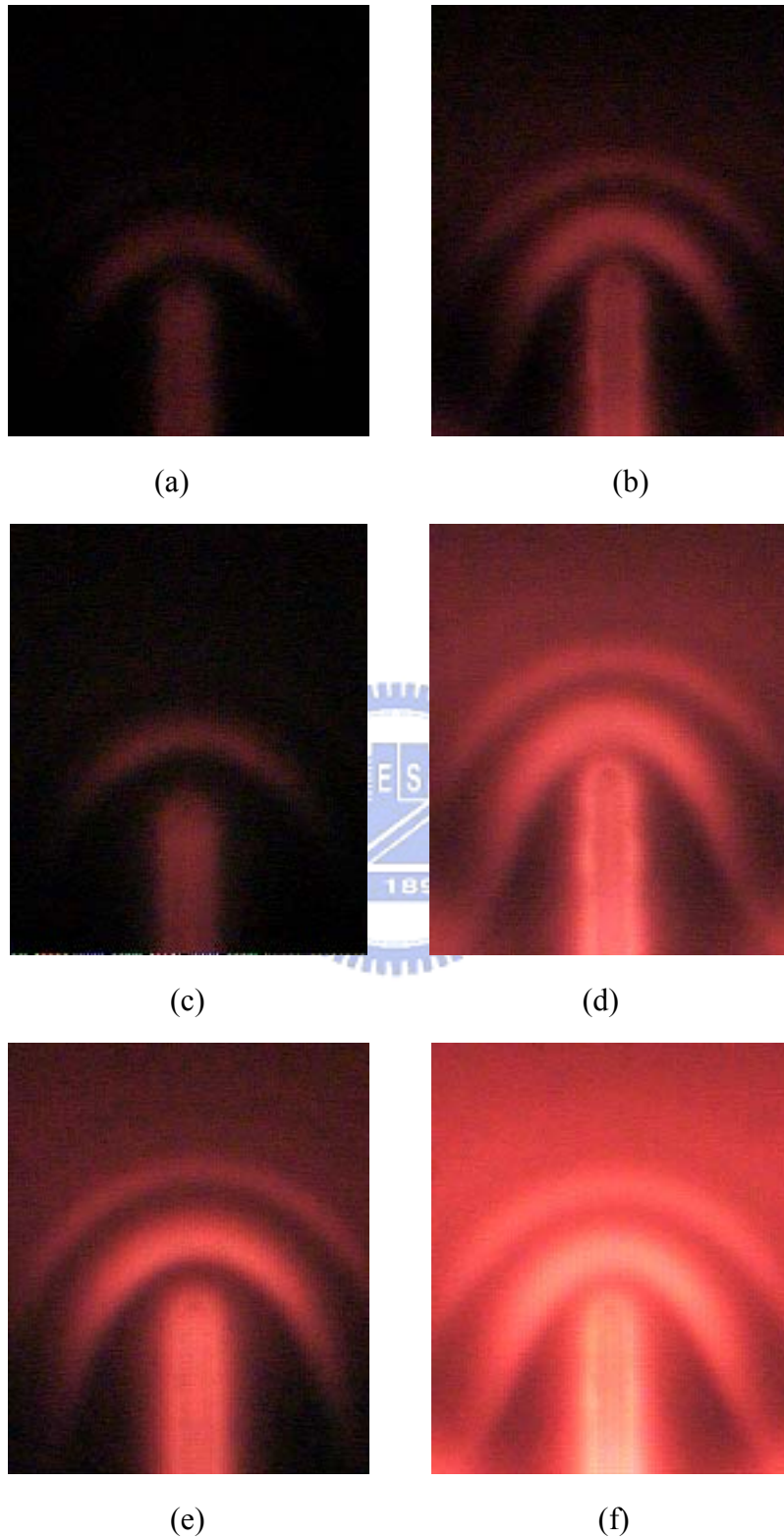
(b)

(c)

(d)

(e)

(f)

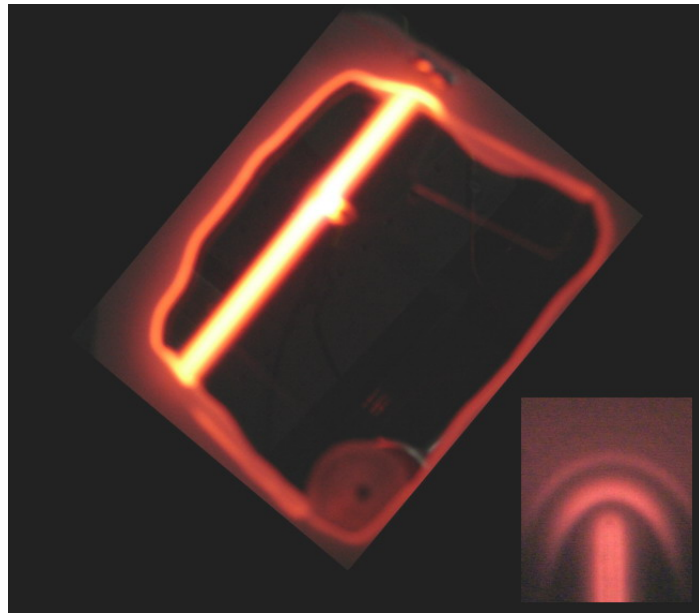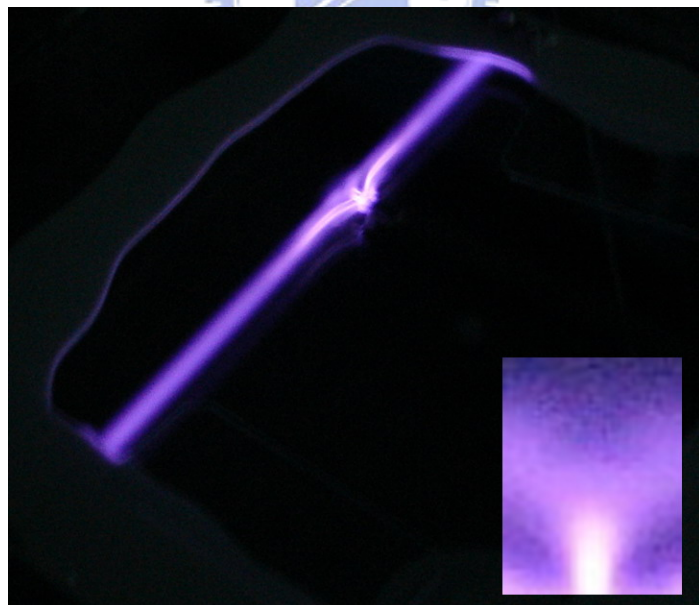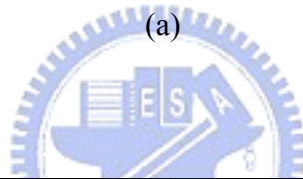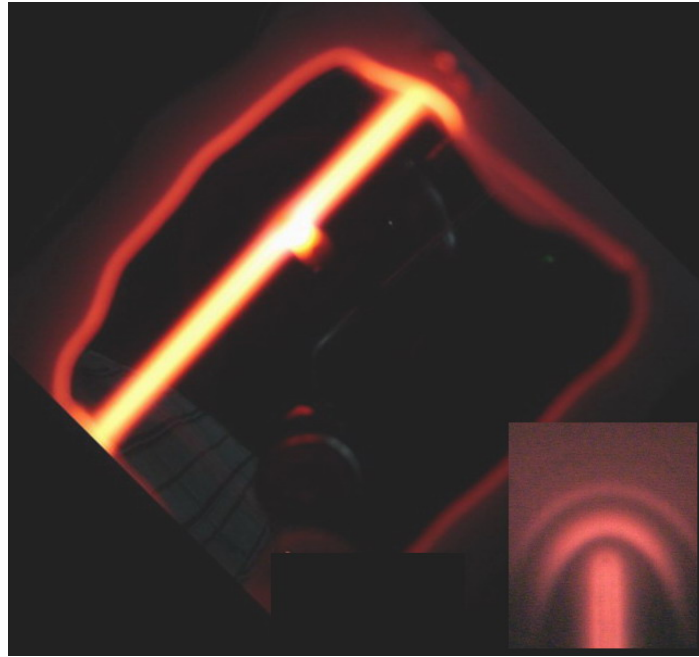Fig. 4-6. CCD images of the glow discharge for the device operating in 400 Torr of neon gas at, (a) 4 kHz, 300 V, (b) 4 kHz, 600 V, (c) 10 kHz, 300 V, (d) 10 kHz, 600 V, (e) 20 kHz, 300 V, (f) 20 kHz, 600 V.
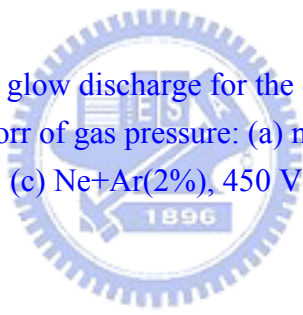
(a)

(b)

(c)

Fig. 4-7. Photographs of the glow discharge for the device operating with 20 kHz pulsed waveform and 400 Torr of gas pressure: (a) neon, 450 V, (b) argon, 500 V, (c) Ne+Ar(2%), 450 V.

Chapter 5

Summary and Future Work

5.1 Summary

High pressure glow discharges stabilized by operating with relatively small characteristic dimensions have been given the term "microplasma". With the intersection of plasma science, photonics and materials science, microplasma device science and technology offers not only a new realm of plasma application but also device capability. The first and second conferences about microplasma are organized in 2003 and 2004 respectively and the third International Workshop on Microplasmas (IWM) is held in Germany, 2006. The growth of this series of microplasma conference shows the developing potential of microplasmas. Recent examples of microplasma devices developed with many configurations, such as inverted pyramid, planar electrode and three dimensional structures. Moreover, materials of microplasma device are also the critical research topics in the development of microplasma device. Research and development on microplasma devices reveal the characteristics which are well-behaved electrically and optically and appear to be valuable and feasible applications such as active display and backlighting [27].

This work was devoted to the characterization of nano-tip enhanced microplasma device in neon, argon and Ne+Ar(2%). Using nano-tip is to locally enhance the electric field and reduce the discharge voltage. This article presents the panel type microplasma devices with nano-tip enhanced electrodes and demonstrates that the

proposed devices have been successfully fabricated and operated with various direct current bipolar pulsed excitation frequencies from 2 to 20 kHz in neon, argon and Ne+Ar(2%) gas mixture. The nano-tip enhanced microplasma devices are characterized by abnormal glow discharge properties and low discharge voltages were acquired due to the fact that the local electric field distribution is heightened by the nano-tips. Operating at pressure up to 800 Torr at voltage as low as 250 V provides stable glow discharge phenomena. Large voltage margin of our proposed devices reveals the potential of wide operating range in future device. Simple fabrication of the devices is an obvious advantage to procure the larger area panel type nano-tip enhanced microplasma devices. The nano-tip enhanced microplasma device technology provides advantages which are discharge voltage, lifetime, brightness, and efficiency. The high resolution patterns with nano-tips, low discharges voltage obtained from the short distance between panel electrodes and the strong emission from the nano-tips can be provided from the proposed devices. Furthermore, with the advantages which are discharge voltage, lifetime, brightness, and efficiency, the nano-tip enhanced microplasma technology provides possible opportunity to integrate with broad applications.

5.2 Future work

Despite the encouraging results of this study as to the positive of using nano-tip enhanced electrodes in the microplasma devices, future research is required in a number of directions. The work we presented is an exciting first step and among the many topics to be explored in future research and some important ones can be discussed as following sections.

5.2.1 Phosphor

In this work, the proposed nano-tip enhanced microplasma device is only one line device. In the future, multi-line and full size panel microplasma device are desired. Because Red, Green, Blue and White (RGBW) colors are desired for display application, vacuum ultra-violet (VUV) excitable phosphors is capable of achieving this future work. To avoid destroying the nano-tip, a spraying method with spray nozzle is commented to grow phosphor layer in the proposed devices. According to the full size panel microplasma device with phosphors, it can provide potential of application on flat plasma light source

5.2.2 Dielectric layer

From the observation of long time operation, there is some erosion which comes from the ion bombardment phenomena on the nano-tip. In order to avoid the erosion, a dielectric layer can be deposited on rear metal electrode to protect the nano-tip enhanced electrode. Base on the plasma display panel (PDP) technology, Magnesium Oxide (MgO) is the best candidate in this future work. MgO can provide low sputtering rate and high secondary emission coefficient. With depositing the MgO thin film, the life time of proposed device is confidently longer.

Reference

[1] K. H. Becker, K. H. Schoenbach and J. G. Eden, "Microplasmas and applications," J. Phys. D: Appl. Phys., **39**, pp. R55-R69, 2006.

[2] A. D. White, "New hollow cathode glow discharge," J. Appl. Phys., **30**, pp. 711-719, 1959.

[3] D. L. Bitzer and H.G. Slottow, "The plasma display panel – a digitally addressable display with inherent memory," AFIPS proceeding, **29**, pp. 541-547, San Francisco, 1966.

[4] Wenhui Shi, Stark, R. H. and Schoenbach, K. H., "Parallel operation of microhollow cathode discharges," Plasma Science, IEEE Transactions on, **27**, pp. 16-17, 1999

[5] Stark R. H., Ernst U., Block R., El-Bandrawy M. and Schoenbach K. H., "Microhollow cathode discharges in atmospheric air," ICOPS'99: IEEE Int. Conf. on Plasma Science, pp. 117, 1999

[6] J. W. Frame, D. J. Wheeler, T. A. DeTemple, J. G. Eden, "Microdischarge devices fabricated in silicon", Appl. Phys. Lett., **71**, pp. 1165-1167, 1997.

[7] J. Gary Eden et al "Microplasma devices fabricated in silicon, ceramic, and metal/polymer structures: arrays, emitters and photodetectors," J. Phys. D: Appl. Phys, **36**, pp. 2869-2877, 2003.

[8] S.-J. Park, J. Chen, C. J. Wagner, N. P. Ostrom, C. Liu and J. Gary Eden, "Microdischarge arrays: A new family of photonic devices," IEEE J. Sel. Topics Quantum Electron, **8,** pp. 387-394, 2002

[9] J. Gary Eden, S.-J. Park, N. P. Ostrom and K.-F. Chen, "Recent advances in microcavity plasma devices and arrays: a versatile photonic platform," J. Phys. D: Appl. Phys, **38**, pp. 1644-1648, 2005.

[10] J. G. Eden et al., "Large array of microcavity plasma devices for active display and backlighting," IEEE/OSA J. Display Tech., **1**, no. 1, pp. 112-116, 2005

[11] J. Gary Eden and S.-J. Park, "Microcavity plasma devices and arrays: a new realm of plasma physics and photonic applications," Plasma Physics and Controlled Fusion, **47**, pp. B83-B92, 2005.

[12] C. Penache, et al., "Micro-structured electrode arrays: A source of high-pressure

non-thermal plasma," <u>Proceedings of SPIE</u>, **4460**, pp. 17-25, 2002.

[13] Yuri P. Raizer, <u>Gas Discharge Physics</u>, Springer-Verlag, Germany, 1991.

[14] Chapman Brian, <u>Glow discharge processes: sputtering and plasma etching</u>, John Wiley & Sons Ltd., New York, 1980.

[15] F. Llewellyn-Jones, <u>Ionization and breakdown in gases</u>, John Wiley & Sons Ltd., New York, 1957.

[16] Nasser Essam, <u>Fundamentals of gaseous ionization and plasma electronics</u>, Wiley-Interscience, New York, 1971.

[17] Franklin Raoul N., <u>Plasma phenomena in gas discharges</u>, Oxford University Press, Oxford, 1977.

[18] Herman V. Boeing, <u>Plasma Science and Technology</u>, Cornell University Press, New York, 1982.

[19] 蘇金春,「氣體放電之研究(Study on Electrical Discharge in Gases)」,國立交通大學,碩士論文,民國四十九年

[20] Homer D. Hagstrum, "Auger ejection of electrons from Molybdenum by noble gas ions," <u>Physical Review</u>, **104**, pp. ,672-683, 1956.

[21] J. L. Vossen and W. Kerns, Eds., <u>Thin Film Processes</u>, Academic, New York, 1978.

[22] L. I. Maissel and R. Glang, "Handbook of Thin film Technology," McGraw-Hill, New York, 1970.

[23] John F. O'Hanlon, <u>A User's Guide to Vacuum Technology</u>, John Wiley & Sons Ltd., New York, 1980.

[24] 蘇青森,<u>真空技術</u>,五版,台北市,台灣東華書局,民國九十一年。

[25] T. Shinoda, H. Uchiike and S. Andoh, "Low-voltage operated AC Plasma-display panels," <u>IEEE Trans. Electron Devices</u>, **ED-26**, pp. 1163-1167, 1979.

[26] C-H Park, Y-K Kim, B-E Park, W-G Lee, and J-S Cho, "Effects of MgO annealing process in a vacuum on the discharge characteristics of AC PDP," <u>Mater. Sci. Engineer B</u>, **B60**, pp. 149-155, 1999.

[27] Rakhwan Kim, Younghyun Kim and J.-W. Park, "Discharge characteristics of MgO and MgO-ZrO$_2$ protective films prepared by electron beam evaporation," <u>Materials Science and Engineering</u>: **B83**, pp. 55-60, 2001.